Semiconductor Measurement Technology

Progress Report
April 1, 1977 to September 30, 1977

NATIONAL BUREAU OF STANDARDS

The National Bureau of Standards[1] was established by an act of Congress on March 3, 1901. The Bureau's overall goal is to strengthen and advance the Nation's science and technology and facilitate their effective application for public benefit. To this end, the Bureau conducts research and provides: (1) a basis for the Nation's physical measurement system, (2) scientific and technological services for industry and government, (3) a technical basis for equity in trade, and (4) technical services to promote public safety. The Bureau's technical work is performed by the National Measurement Laboratory, the National Engineering Laboratory, and the Institute for Computer Sciences and Technology.

THE NATIONAL MEASUREMENT LABORATORY provides the national system of physical and chemical and materials measurement; coordinates the system with measurement systems of other nations and furnishes essential services leading to accurate and uniform physical and chemical measurement throughout the Nation's scientific community, industry, and commerce; conducts materials research leading to improved methods of measurement, standards, and data on the properties of materials needed by industry, commerce, educational institutions, and Government; provides advisory and research services to other Government agencies; develops, produces, and distributes Standard Reference Materials; and provides calibration services. The Laboratory consists of the following centers:

Absolute Physical Quantities[2] — Radiation Research — Thermodynamics and Molecular Science — Analytical Chemistry — Materials Science.

THE NATIONAL ENGINEERING LABORATORY provides technology and technical services to the public and private sectors to address national needs and to solve national problems; conducts research in engineering and applied science in support of these efforts; builds and maintains competence in the necessary disciplines required to carry out this research and technical service; develops engineering data and measurement capabilities; provides engineering measurement traceability services; develops test methods and proposes engineering standards and code changes; develops and proposes new engineering practices; and develops and improves mechanisms to transfer results of its research to the ultimate user. The Laboratory consists of the following centers:

Applied Mathematics — Electronics and Electrical Engineering[2] — Mechanical Engineering and Process Technology[2] — Building Technology — Fire Research — Consumer Product Technology — Field Methods.

THE INSTITUTE FOR COMPUTER SCIENCES AND TECHNOLOGY conducts research and provides scientific and technical services to aid Federal agencies in the selection, acquisition, application, and use of computer technology to improve effectiveness and economy in Government operations in accordance with Public Law 89-306 (40 U.S.C. 759), relevant Executive Orders, and other directives; carries out this mission by managing the Federal Information Processing Standards Program, developing Federal ADP standards guidelines, and managing Federal participation in ADP voluntary standardization activities; provides scientific and technological advisory services and assistance to Federal agencies; and provides the technical foundation for computer-related policies of the Federal Government. The Institute consists of the following centers:

Programming Science and Technology — Computer Systems Engineering.

[1] Headquarters and Laboratories at Gaithersburg, MD, unless otherwise noted;
mailing address Washington, DC 20234.
[2] Some divisions within the center are located at Boulder, CO 80303.

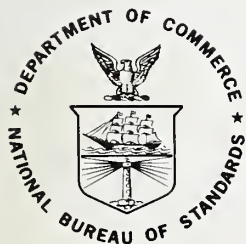# Semiconductor Measurement Technology
April 1, 1977 to September 30, 1977

W. Murray Bullis, Editor

Electron Devices Division
Center for Electronics and Electrical Engineering
National Engineering Laboratory
National Bureau of Standards
Washington, D.C. 20234

National Bureau of Standards Special Publication 400-45

Nat. Bur. Stand. (U.S.), Spec. Publ. 400−45, 43 pages (Aug. 1980)

CODEN: XNBSAV

TABLE OF CONTENTS

SEMICONDUCTOR MEASUREMENT TECHNOLOGY

LIST OF FIGURES

LIST OF TABLES

Page

PREFACE

The Semiconductor Technology Program serves to focus NBS research to enhance the performance, interchangeability, and reliability of discrete semiconductor devices and integrated circuits through improvements in measurement technology for use in specifying materials and devices in national and international commerce and for use by industry in controlling device fabrication processes. This research leads to carefully evaluated and well-documented test procedures and associated technology. Special emphasis is placed on the dissemination of the results of the research to the electronics community. Application of these results by industry will contribute to higher yields, lower cost, and higher reliability of semiconductor devices. Improved measurement technology also leads to greater economy in government procurement by providing a common basis for the purchase specifications of government agencies, and, in addition, provides a basis for controlled improvements in fabrication processes and in essential device characteristics.

During this reporting period, the Program received direct financial support principally from two major sponsors: the Defense Advanced Research Projects Agency (ARPA)[*] and the National Bureau of Standards (NBS)[†] and, in addition, from the Defense Nuclear Agency (DNA),[§] the Navy Strategic Systems Project Office,[¶] the Energy Research and Development Administration,[#] and the Naval Ocean Systems Center.[×] The ARPA-supported portion of the Program, Advancement of Reliability, Processing, and Automation for Integrated Circuits with the National Bureau of Standards (ARPA/IC/NBS), addresses critical Defense Department problems in the yield, reliability, and availability of digital monolithic integrated circuits. Other portions of the Program emphasize aspects of the work which relate to the specific needs of the supporting agency. Measurement-oriented research appropriate to the mission of NBS is an essential aspect in all parts of the Program.

Essential assistance to the Program is also received from the semiconductor industry through cooperative experiments and technical exchanges. NBS interacts with industrial users and suppliers of semiconductor devices through participation in standardizing organizations; through direct consultations with device and material suppliers, government agencies, and other users; and through scheduled symposia and workshops. In addition, detailed reports such as state-of-the-art reviews, literature compilations, and summaries of technical efforts conducted within the Program are issued as these activities are completed. Major reports of this type which are published by NBS appear in the Special Publication 400- subseries.

Another means of interaction with the electronics community is by direct contact. In particular, comments from readers regarding the usefulness of the results reported herein or relating to directions of future activity in the Program are always welcome.

SEMICONDUCTOR MEASUREMENT TECHNOLOGY

PROGRESS REPORT
April 1, 1977 to September 30, 1977

Abstract: This progress report describes NBS activities directed toward the development of methods of measurement for semiconductor materials, process control, and devices. Both in-house and contract efforts are included. The emphasis is on silicon device technologies. Principal accomplishments during this reporting period included (1) development of theoretical expressions for computing resistivity and hole mobility for boron-doped silicon; (2) completion of a study of problems associated with use of a scanning electron microscope for total dose testing of semiconductor devices; (3) completion of a pilot study to evaluate procedures for measuring 1- to 10-μm wide clear and opaque lines viewed with transmitted illumination; (4) completion of a preliminary study of test structures for estimating densities of process-induced random faults in device wafers; and (5) completion of an interlaboratory evaluation of the destructive wire-bond pull test. Also reported is other ongoing work on materials characterization by electrical and physical analysis methods, materials and procedures for wafer processing, photolithography, test patterns, and device inspection and test procedures.

Key Words: Capacitance-voltage methods; deep level transient spectroscopy; electrical properties; electron irradiation; electronics; hole mobility; integrated circuits; ion knock-on effect; ion microprobe mass analysis; Irvin's curves; isothermal transient capacitance method; linewidth measurements; measurement technology; microelectronics; phosphorus pileup; photolithography; pull test; random fault test structures; resistivity; scanning acoustic microscope; scanning electron microscope; semiconductor devices; semiconductor materials; semiconductor process control; silicon; silicon dioxide; spatial filtering microscope; sputter-Auger method; test structures; transistors; wire bonds.

1. INTRODUCTION

This is a report to the sponsors of the Semiconductor Technology Program on work carried out during the thirty-sixth and thirty-seventh quarters of the Program. The report summarizes research on a wide variety of measurement methods for semiconductor materials, process control, and devices that are being studied at the National Bureau of Standards (NBS). The Program, which emphasizes silicon-based device technologies, is a continuing one, and the results and conclusions reported here are subject to modification and refinement.

The Program is divided into a number of task areas, each directed toward the study of a particular material or device property or measurement technique. This report is subdivided according to these tasks. Highlights of activity during the reporting period are given in section 2. This section provides a management-level overview of the entire effort.

Subsequent sections deal with each specific task area. The report of each task includes a narrative description of progress made during this reporting period. References cited are listed in the final section of the report. Affiliations of staff members identified with each task are those during the reporting period; unless otherwise identified, staff were affiliated with the Electronic Technology Division. These affiliations are given for record purposes only; many changes

have occurred because of a reorganization of the NBS which took place on April 19, 1978.

Background material on the Program and individual tasks may be found in earlier progress reports as listed in the Appendix. From time to time, publications are prepared that describe some aspect of the program in greater detail. Because of the long delay between the end of the reporting period and the publication of this report, reports of this type are not listed herein. A complete listing of publications issued by the Program is available in NBS List of Publications LP72, Semiconductor Measurement Technology.

This is the last of these comprehensive progress reports. Work carried out after October 1, 1977 is reported in condensed form under the title, Semiconductor Technology Program, Progress Briefs, in the NBSIR series. These Progress Briefs also contain listings of more detailed publications printed during the reporting period covered or scheduled for publication in the near future.

Additional information concerning the projects described in this report, information on current projects, and copies of List of Publications LP72 or of current issues of Progress Briefs can be obtained on request to Electron Devices Division, National Bureau of Standards, Washington, D.C. 20234, telephone (301) 921-3786.

1

2. HIGHLIGHTS

Highlights of progress in the various technical task areas of the Program are listed in this section. Particularly significant accomplishments during this reporting period included:

(1) development of theoretical expressions for computing resistivity and hole mobility for boron-doped silicon;

(2) completion of a study of problems associated with use of a scanning electron microscope for total dose testing of semiconductor devices;

(3) completion of a pilot study to evaluate procedures for measuring 1- to 10-μm wide clear and opaque lines viewed with transmitted illumination;

(4) completion of a preliminary study of test structures for estimating densities of process-induced random faults in device wafers; and

(5) completion of an interlaboratory evaluation of the destructive wire-bond pull test.

Unless another organization is identified, the work described in the following paragraphs was performed at the National Bureau of Standards.

Materials Characterization by Electrical Methods — Work continued on the experimental redetermination of the resistivity–dopant density (ρ–N) relations for silicon (Irvin's curves). Because the impurities in silicon are not fully ionized at room temperature in the intermediate dopant density range, the dopant density (N) is not always equal to the carrier density (n). It was found to be convenient to display the results of this work in the form of the product $q\rho N$ (or its reciprocal) against N or ρ as well as in the form of mobility (the reciprocal of $q\rho n$) against n or ρ.

Theoretical expressions were derived for the resistivity and hole mobility as functions of dopant density and temperature in boron-doped silicon. The model upon which the expressions are based is applicable for dopant densities from 10^{13} to 3×10^{18} cm^{-3} and for temperatures from 100 to 400 K. This project was carried out at the University of Florida.

An analytical study of the validity of the models used in analyzing differential capacitance impurity profiling measurements was undertaken with the identification of several critical problems.

The isothermal transient capacitance (ITCAP) technique was extended to combine the use of a commercial 1-MHz capacitance bridge with the repetitively pulsed charging technique used in deep level transient spectroscopy. The extension allows more rapid data analysis and the measurement of shorter emission decay rates than can be achieved with the conventional ITCAP method.

In addition, a detailed analysis of the isothermal initial and final capacitance method demonstrated that this method, in conjunction with the conventional ITCAP method, can be used for distinguishing between the majority and minority carrier emission rates of mid-gap defect centers.

Materials Characterization by Physical Analysis Methods — As part of an ongoing task at Texas Instruments to develop methods for preparation of standards for calibrating an ion microprobe mass analyzer (IMMA), an experiment was carried out to estimate the repeatability of the IMMA. Measurements were made over periods ranging from about 15 min to 1 week. The average relative sample standard deviations for all measurement series were less than 7.5 percent.

Several thermally oxidized phosphorus-doped silicon wafers were examined to determine if the width of the oxide-silicon interface as measured by the sputter-Auger method is affected by the presence of the large concentrations of phosphorus which pile up on the silicon side of the interface during oxidation. The measured interface width was found to increase significantly with increased phosphorus density.

In a related project, a simple model, based on an analogy to thermal diffusion theory, was developed to account for ion knock-on broadening during sputter-Auger profiling. These activities were carried out at Stanford University.

A study of the problems associated with the use of a scanning electron microscope (SEM) to simulate a gamma source such as cobalt-60 for total dose testing of semiconductor devices was completed. It was concluded that the SEM can serve as a convenient tool for this purpose if attention is given to several critical factors.

Photolithography — The initial three-laboratory pilot study of procedures for mea-

suring 1- to 10-μm wide clear and opaque lines viewed with transmitted light was completed. The results showed wide variations between various participating groups and indicated that some of the systematic errors introduced into the measurement cannot be eliminated by a simple two-point calibration technique. An artifact with a new pattern has been designed so that appropriate calibration data can be determined.

The analysis of the spatial filtering microscope was extended to the case of a single edge. It was shown that any band-pass filter provides accurate edge location (in the form of a sharp minimum at the edge position) provided there is sufficient energy left in the image for observation.

An improved model was developed to describe the interaction of an electron beam with a line edge. Although this model does not consider either "bloom" of the electron beam or fairing and rounding at the top and bottom of the real edge, the model appears to provide a reasonably satisfactory basis for locating the edge.

Satisfactory measurements of a chromium-on-glass pattern of 0.5-μm wide lines and spaces were made with the scanning photometric microscope operating in transmitted light. Operation in reflected light was hampered by lack of adequate source intensity; a krypton laser source is being incorporated into the system to overcome this limitation.

Test Patterns — Preliminary evaluations were conducted of random fault test structures for determining defect densities related to metal step coverage, contacts to resistors, and multi-emitter transistors. Various methods for estimating defect densities were compared; it was found that good estimates of defect density could be obtained from limited data when the test structure has a number of elements such that one (but not more than one) defect occurs in a reasonable fraction

of the structures. Measurements on five test sites on a wafer were found to be inadequate to provide a reasonable estimate.

Assembly and Packaging — Analysis of an interlaboratory evaluation of the destructive wire bond pull test was completed. Problems with calibration of a widely used pull tester were identified; these were subsequently corrected by the manufacturer. Satisfactory agreement was obtained except for one group of bonds which had been intentionally poorly made and overly deformed. The test results support the conclusion that the permitted bond deformation should not exceed two wire diameters for aluminum wire bonds.

Device Inspection and Test — It was observed that when a polished surface of a single crystal is examined with a converging acoustic beam, the reflected signal has a characteristic response that is dependent upon the elastic properties of the reflecting surface. This property can be used in the scanning acoustic microscope to monitor the thickness of films deposited on these surfaces.

Preliminary results of experiments to study the resolution of the scanning acoustic microscope showed that a periodic pattern of 2-μm wide lines and spaces could be resolved at an operating frequency of 750 MHz and that both this pattern and a periodic pattern of 1-μm wide lines and spaces could be resolved at an operating frequency of 1100 MHz.

The feasibility of a reflective acoustic ten-step gray scale for use with a scanning acoustic microscope operated at 375 MHz was demonstrated although the dynamic range is quite limited. The gray scale employs a single contoured layer of light borate crown glass on a sapphire substrate.

The gray-scale project was carried out at Hughes Research Laboratories, and the other scanning acoustic microscope projects were carried out at Stanford University.

3. MATERIALS CHARACTERIZATION BY ELECTRICAL METHODS

3.1. Reevaluation of Irvin's Curves

Carrier mobility is frequently calculated from measurements of resistivity and dopant density. However, such calculations are correct only when the carrier density, n, is equal to the dopant density, N. At room temperature, the two are generally not equal in the dopant density range from about 10^{17} cm^{-3} to about 10^{19} cm^{-3} because of incomplete ionization of the dopant atoms (NBS Spec. Publ. 400-19, pp. 13-16). For example, for silicon doped with phosphorus to a density of about 10^{18} cm^{-3}, it is estimated that only 85 to 90 percent of the phosphorus atoms are ionized [1,2]. For silicon doped with boron to about the same density, it is estimated that 70 to 80 percent of the boron atoms are ionized [3,4]. This difference occurs because, even though boron and phosphorus have essentially the same ionization energy, the effective masses of the majority carriers and the degeneracy factors for the impurity levels are different in the two cases. Other n-type dopants, such as arsenic and antimony have nearly the same ionizaton fraction as phosphorus, but for other p-type dopants, such as gallium and indium, the percent ionization at a given dopant density is smaller because of the larger ionization energies of these dopants [5].

Thus, the quantity $1/q\rho N$, where q is the electron charge and ρ is the resistivity, yields the mobility only when N = n. This assumption is frequently made. The Caughey-Thomas [6] mobility expressions, which are fits to the Irvin [7] curves, are based both on data from Hall effect measurements, which give carrier density within the uncertainty of the Hall scattering factor, and on data from chemical techniques which give the total dopant density; no distinction between the two was made. Likewise, Mousty *et al.* [8] did not include deionization effects in their work on phosphorus-doped silicon. Both Hall effect and neutron activation analysis data were plotted as phosphorus density. Differences between the two were attributed solely to the Hall scattering factor. Wagner [9] obtained an expression for hole mobility based on measurements on silicon implanted with boron. The amount of boron retained in the silicon was determined by integration of data obtained from incremental sheet resistance and Hall effect measurements on layers which were sectioned by anodic oxidation. A mobility value as a function of boron density

was derived which made the integrated dose equal to the implanted dose. This is equivalent to the assumption that all of the boron was electrically active and ionized.

There is a need for curves and analytical expressions to relate resistivity to both carrier density and dopant density. It is convenient to use the mobility ($\mu = 1/q\rho n$) and the quantity $1/q\rho N$ (or its reciprocal) to relate resistivity to carrier density and dopant density, respectively, since these quantities exhibit details and structure not easily displayed on a ρ-N or ρ-n plot which must generally cover many decades. Equilibrium cases involve the use of mobility as a function of carrier density. For example, consider the determination of a dopant density profile of a diffused layer from incremental sheet resistance measurements [10]. The resistivity values are converted to carrier density using knowledge of the mobility as a function of carrier density. Then dopant density is calculated from carrier density using information on percent ionization. Depletion conditions, under which the dopant atoms are fully ionized, involve the use of curves of $1/q\rho N$ as a function of dopant density. Examples include the determination of the resistivity of the specimen from measurements of voltage breakdown or of capacitance as a function of applied voltage.

(W. R. Thurber)

3.2. Hole Mobility in p-Type Silicon

Theoretical expressions for computing resistivity and conductivity of holes as functions of dopant density and temperature were derived for boron-doped silicon. The model is applicable for dopant densities from 10^{13} to 3×10^{18} cm^{-3} and temperatures, T, between 100 and 400 K [3,4].

Using a 3-band [i.e., heavy-hole, light-hole, and spin-orbit split-off (SOS) bands] model, the hole mobility was calculated by properly combining the contributions from scattering by lattice phonons, ionized impurities, and neutral impurities. In addition, the effect of hole-hole (h-h) scattering and the nonparabolicity of the valence bands were taken into account in the mobility formulation.

To verify the theoretical calculations, resistivity measurements on nine boron-doped silicon slices with dopant densities from 4.5

$\times 10^{14}$ to 6×10^{18} cm^{-3} were performed for $100 \leq T \leq 400$ K, using a planar square-array test structure [11]. Agreement between the calculated and measured resistivity values was within 6 percent over the entire range of dopant density and temperature studied here. Excellent agreement (within ±5 percent) between the calculated hole mobility values and those of Wagner [9] was obtained for boron densities less than 10^{17} cm^{-3}. Differences found for boron densities greater than 10^{17} cm^{-3} are attributed to Wagner's neglect of the effect of the deionization of boron atoms in this dopant range (see sec. 3.1.).

(S. S. Li*)

3.3. Capacitance-Voltage Methods

An analytical study of the theoretical validity of the differential capacitance impurity profiling method was undertaken. In the initial phase, the following problems and questions related to successful application of the method were identified:

1. The Schottky equations, which form the foundation of the classical differential capacitance method, are strictly only valid for one-sided junctions [12,13,14]. What kind of errors does this cause in practical applications?

2. Are the claims that the Schottky equations profile the equilibrium majority carrier density near a junction rather than the impurity distribution [15,16] correct? How can the seemingly conflicting answers [17,18] to these claims be resolved?

3. A method has been suggested for theoretically testing the validity of the Schottky equations [15,16]. This method does not depend on the depletion layer approximation but does formally depend on the theoretical equations one uses in carrying through the calculations. This raises the question of whether one should use the electron-hole transport equations with recombination-

generation terms or the Poisson-Boltzmann equation. Also, the results of applying the testing method depend on the choice used in defining capacitance and depletion layer width. What are the proper definitions [19,20,21] for these quantities in more exact theories than the depletion layer approximation? (S. R. Kraft[†])

3.4. Thermally Stimulated Current and Capacitance Measurements[§]

Transient Capacitance Technique [22] — Several methods for the detection of deep level defects in semiconductors by the measurement of depletion capacitance transients have been utilized by a number of investigators [23-28]. In the traditional thermally stimulated capacitance (TSCAP) measurement [23,24], defects charged at low temperatures are induced to discharge by heating the device. In the deep level transient spectroscopy (DLTS) technique [25], the device is repeatedly pulsed to charge the defect, and the discharge during a fixed time interval is monitored as the device temperature is changed slowly. In a third technique, the isothermal transient capacitance (ITCAP) technique (NBS Spec. Publ. 400-36, pp. 20-22) [26], the discharge transient is observed directly after the device has been switched from charging bias to depletion bias at a fixed temperature. Whereas DLTS typically utilizes a 20-MHz bridge [27] for measurement of capacitance, both TSCAP and ITCAP are typically performed with a commercial 1-MHz capacitance bridge. All three methods are capable of determining the density, energy level, and emission rate of the defect.

The ITCAP method was extended to combine the use of the commercial 1-MHz capacitance bridge with the repetitively pulsed charging technique. A digital processing oscilloscope (DPO) is used in conjunction with a minicomputer to capture the capacitance transient and perform computations to characterize it. This extension allows rapid data analysis and the measurement of shorter emission decay rates than can be achieved with the conventional ITCAP method. In addition, it permits rapid measurements to facilitate wafer mapping of defect densities (NBS Spec. Publ. 400-38, pp. 10-12).

Figure 1 shows a typical series of bias pulses and the resulting capacitance transients. A $p^{+}n$ junction structure is assumed for specificity and only majority carrier charging [25] is assumed for simplicity.
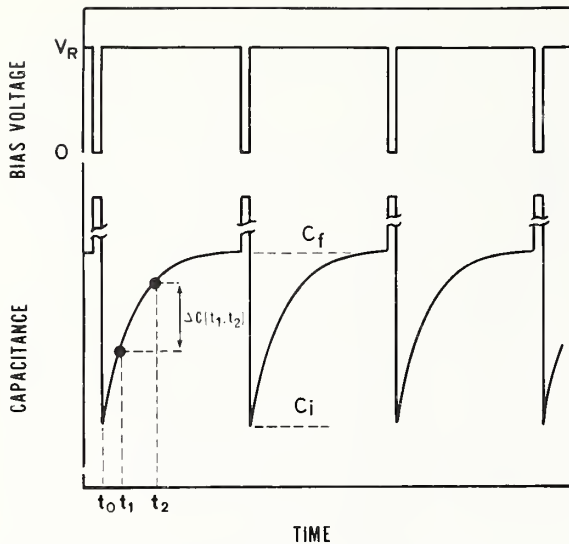
Figure 1. Schematic presentation of (a) the pulsed applied voltage and (b) the resulting capacitance transient.

The large capacitance pulse accompanying the zero-bias voltage pulse is due to the momentary collapse of the depletion region which allows charging of the traps. After re-establishing depletion, the charged traps emit carriers at a rate governed by the temperature, and the initial capacitance, C_i, decays exponentially to a final value of capacitance, C_f:

$$C(t,T) = C_f - (C_i - C_f) \exp(-et) \qquad (1)$$

where $C(t,T)$ is the capacitance at time t and temperature T and e is the emission rate. In the DLTS mode of operation, the difference in capacitance at fixed times t_1 and t_2 after depletion is reestablished is monitored as a function of temperature. This is typically done with a dual-channel box car integrator.

In the usual ITCAP measurement, a single capacitance transient is captured on a recording medium such as an x-y recorder. The response time of the recorder and the background noise level generally limit this measurement to transient times in excess of 100 ms. In the modified ITCAP technique, the device under test is maintained at a fixed temperature, but it is repetitively pulsed as in the DLTS mode. The dc depletion bias is applied to the device via the "LO BIAS" input of the commercial 1-MHz capacitance bridge, as shown in the block diagram in figure 2. The charging pulses are applied in series with the device via a pulse transformer on the "LO" side of the input. In order to

utilize the useful dynamic range of the digital processing oscilloscope fully, it is necessary and desirable to suppress the large zero-bias capacitance pulse which precedes the transient capacitance signal. This is simply accomplished by suitably gating the analog output of the capacitance bridge.

Figure 3 shows three typical signals obtained while studying a gold-doped p^+n device which was held at a -15 V reverse bias and pulsed to zero bias with a 1-μs pulse. The signal applied to the analog gate (a) appears at the point marked ① in figure 2. The gate width is adjusted to blank out the input of the DPO during the large zero-bias capacitance pulse,[¶] which dominates the ungated analog signal (b) which appears at point ② in figure 2. The width of this capacitance pulse is indicative of the response time of the capacitance bridge, generally less than 1 ms. Note that the negative-going capacitance transient is barely observable in this trace. The gated capacitance transient (c) appears at point ③ in figure 2. The signal-to-noise ratio for each of the three traces in figure 3 was enhanced by averaging the signal over 100 transients by use of the capabilities of the DPO and its associated minicomputer. Note that in adjusting the repetition period of the applied pulses, it is necessary to insure that equilibrium to C_f has, in fact, been established.

The signal-to-noise ratio can be improved by averaging over more transients. Figure 4 shows the full gated capacitance transient, both a single trace and the average over some 2000 transients. The latter trace can be analyzed to obtain the emission rate, shown in figure 5. The relative "flatness" of the calculated emission rate is indicative of the true exponential behavior of the curve. The increase in noise as a function of time is due to the statistical increase in the uncertainty of the signal as the transient gets smaller with time. The absence of the differential discontinuity at the beginning of the transient and the abrupt zero near the end of the transient are due to software manipulations to avoid overdriving the dynamic range of the processor. A value for the emission rate is obtained simply by taking an average over the relevant range. In this case, the emission rate is calculated to be

---

[¶] The adjustable gate delay is convenient for setting of the gate position when a pulse generator which has an adjustable delay time between the sync and gate pulses is employed.
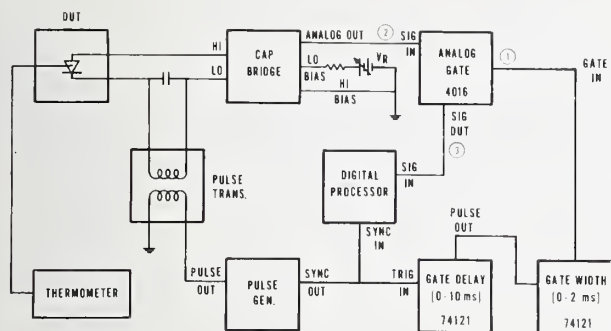
Figure 2. Block diagram for the pulsed iso-thermal transient capacitance measurement.
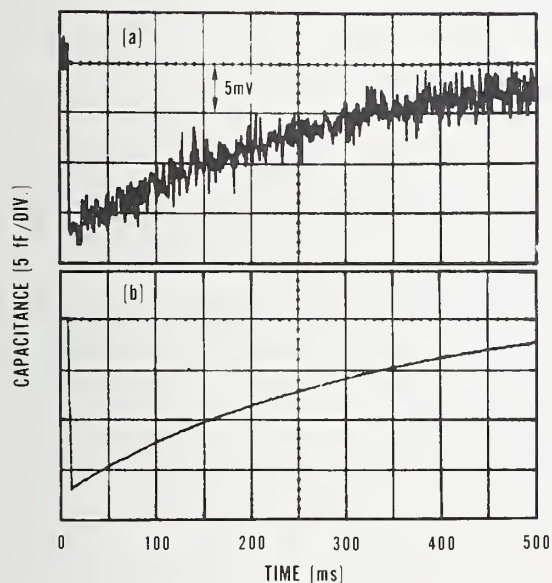
Figure 4. Oscilloscope traces of (a) a single-gated capacitance transient and (b) the gated capacitance transient averaged 2000 times.

Figure 3. Oscilloscope traces of (a) the gate pulse, (b) the ungated capacitance transient, and (c) the gated capacitance transient. (Each trace is the average of 100 scans.)
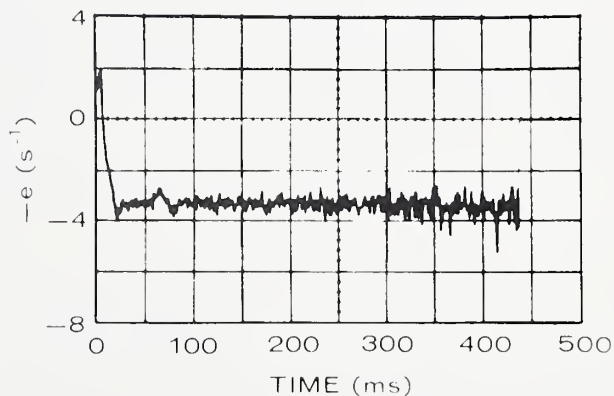
Figure 5. Oscilloscope trace of the calcu-lated emission rate.

3.3 s^{-1} at a temperature of 238 K; this value is in good agreement with the data of Sah *et al.* [28] for electron emission from the gold acceptor.   (R. Y. Koyama)

Analysis of Mid-Gap Levels — Characterization of some mid-gap defect centers requires dis-tinguishing between majority and minority carrier emission rates. Analysis of isother-mal capacitance transient response measure-ments (NBS Spec. Publ. 400-36, pp. 20-22) yields the sum of the majority and minority

carrier emission rates of the defect cen-ters:

$$e = e_n + e_p , \qquad (2)$$

where e_p is the hole emission rate and e_n is the electron emission rate. For those de-fect centers whose electron and hole emission rates are nearly equal, additional measure-ments are required to completely characterize the defect center.

7

The isothermal initial and final capacitance method [26] was analyzed to determine its applicability for this purpose [29]. Under conditions for which the defect center energy level is several kT from the Fermi level (where k is the Boltzmann constant), the defect centers of a reverse-biased junction can be fully charged initially by removing the reverse bias. Then the initial net space-charge density on the n-side of a p^+n junction is [26]

$$N_d - N_t = (2V/q\epsilon A^2)/(C_i^{-2} - C_b^{-2}) , \qquad (3a)$$

and on the p-side, where the defect centers are not charged, it is

$$N_d = (2V/q\epsilon A^2)/(C_i^{-2} - C_b^{-2}) , \qquad (3b)$$

where N_d is the dopant (net acceptor or donor density), N_t is the defect density, V is the change in bias voltage from the applied bias value to the charging (zero) bias, q is the electronic charge, ϵ is the dielectric constant of silicon, A is the junction area, C_i is the initial junction capacitance (with defect center charged), and C_b is the unbiased junction capacitance. The capacitance decays in accordance with eq (1); a representative capacitance transient is shown in figure 6. After discharge, the defect centers return to their steady-state charge density, and the net space-charge density on the n-side of a p^+n junction becomes

$$N_d - [N_t e_p/(e_n+e_p)] = (2V/q\epsilon A^2)/(C_f^{-2}-C_b^{-2}) \quad (4a)$$

and on the p-side

$$N_d + [N_t e_n/(e_n+e_p)] = (2V/q\epsilon A^2)/(C_f^{-2}-C_b^{-2}) \quad (4b)$$

where C_f is the final (steady-state) junction capacitance. Subtraction of eq (4a) from eq (3a) or eq (4b) from eq (3b) gives the same result [26]:

$$\frac{N_t e_n}{e_n + e_p} = \frac{2V}{q\epsilon A^2} \frac{C_b^2(C_f^2 - C_i^2)}{(C_b^2 - C_f^2)(C_b^2 - C_i^2)} . \qquad (5)$$

This can be arranged to give the ratio of hole to electron emission rates in the p^+n junction:

$$\frac{e_p}{e_n} = \frac{N_t q\epsilon A^2}{2V} \frac{(C_b^2 - C_f^2)(C_b^2 - C_i^2)}{C_b^2(C_f^2 - C_i^2)} - 1 . \qquad (6)$$
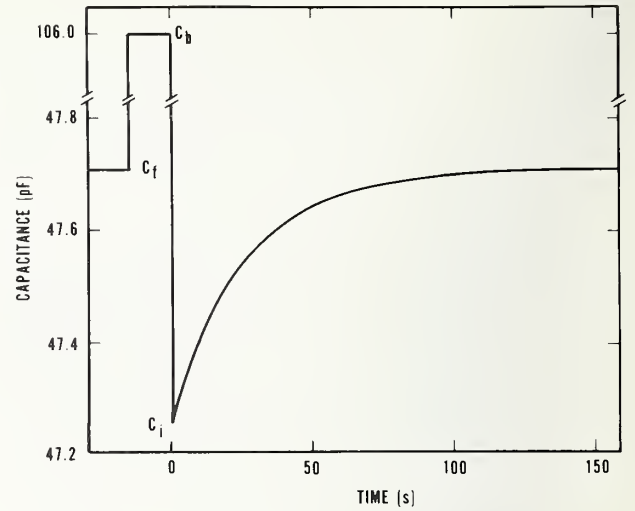
Figure 6. Representative isothermal transient capacitance response of a reverse-biased p^+n junction. (Device 87AN9.1 at 226.66 K with bias of -5 V.)

Hence, e_n and e_p are separable by combining eq (6) and eq (2) (with e determined from isothermal capacitance transient measurements).

An independent, accurate measurement of N_t is required to evaluate e_p/e_n. The ratio N_d/N_t can be obtained from a dynathermal thermally stimulated capacitance measurement [30], and N_d can be determined from the resistivity of the lightly doped side of the junction. It is the fractional uncertainty of the N_t determination which places a lower limit on the value of the e_p/e_n ratio which can be reliably determined. The emission rates can be expressed in terms of the empirical equation of Arrhenius as

$$e_x = B_x T^a \exp(-\Delta E_x/kT) , \qquad (7)$$

where x is either n or p, ΔE_n is the energy difference between the defect center and the conduction band and ΔE_p is the energy difference between the defect center and the valence band. The prefactor $B_n T^a$ or $B_p T^a$ is equal to the product of the electron or hole thermal velocity, the electron or hole capture cross section, and the density of states in the conduction or valence bands, respectively. When $\Delta E_x \gg kT$, the exponential term dominates the variation with temperature. Present experimental precision is inadequate to distinguish between various small values of the temperature exponent in

8

the prefactor; the frequently made choice of $a = 2$ results from the assumption of a temperature-independent capture cross section.

With e_n and e_p known at several temperatures, Arrhenius plots of the natural logarithm of e_n/T^2 and e_p/T^2 against reciprocal temperature, T^{-1}, can be made. Each plot has a slope of $-\Delta E_x/k$ and an intercept of $\ln B_x$. It is expected that the isothermal capacitance transient, initial and final capacitance, and dynathermal capacitance measurements will be adequate to characterize the majority and minority carrier emission rates of a defect center. (W. E. Phillips)

4. MATERIALS CHARACTERIZATION BY
PHYSICAL ANALYSIS METHODS

4.1. Calibration Standards for Ion Microprobe Mass Analysis

As part of a task to develop methods for preparation of standard specimens for empirically calibrating an ion microprobe mass analyzer (IMMA) (NBS Spec. Publ. 400-19, pp. 20-22), an experiment to estimate the repeatability of the IMMA was carried out. A bulk sample of phosphorus-doped silicon with a nominal room temperature resistivity of 0.004 $\Omega \cdot$cm (equivalent phosphorus density, 1.6 $\times$ 10^{19} cm^{-3}) served as the test specimen.

A 22-nA, 19.4-keV ^{32}O$^+$ ion beam was used to analyze the test specimen. The beam was rastered over an area nominally 125 μm by 100 μm, and a 42-μm by 33-μm aperture was employed. Counts were made of the ^{31}P and ^{30}Si secondary ions. The beam was electrostatically switched each 100 ms until a total of 10 s of counting time had been accumulated for each isotope, and a ^{31}P/^{30}Si count ratio was computed. This took 22 s of elapsed time (10 s for ^{31}P counting, 10 s for ^{30}Si counting, and 2 s for switching). Generally, 25 to 50 count ratios were taken in each run to obtain a statistically meaningful sample.

To estimate the short-term ($\sim$15-min) repeatability, 7 runs were made and each was analyzed to obtain the mean value of the ^{31}P/^{30}Si count ratio and the relative sample standard deviation (RSSD) for the run. The average RSSD was 7.4 percent with a sample standard deviation of 1.1 percent.

To estimate the intermediate-term ($\sim$2- to 4-h) repeatability, 3 sets of data, comprising 3 to 8 runs each, were analyzed. In this case, each datum was the average of 25 to 50 count ratios. The mean and RSSD of these averages were computed for each set of data. The average RSSD was 3.2 percent with a sample standard deviation of 1.0 percent.

To estimate the longer term (7-day) repeatability, 10 runs were made during the period July 11 to July 18, 1977. Runs were made during the afternoon of the first day, the morning and afternoon of the next four days, and the afternoon of the last day. The count ratios were analyzed to obtain the mean value (1.113 $\times$ 10^{-3}) and RSSD (6.1%). An analysis of this same specimen about 18 months earlier yielded a count ratio of 1.249 $\times$ 10^{-3}, a value only about 12 percent higher than was obtained in the present series.

It should be noted that differences in count ratios obtained in different runs may reflect microinhomogeneities in the silicon slice because a new 125-μm by 125-μm area was used for each run. The doping uniformity on this scale is not known for this particular slice, but silicon slices with dopant densities suitable for measurement with the IMMA cannot be obtained with microresistivity variations smaller than 5 to 10 percent.

(R. Dobrott* and G. B. Larrabee*)

4.2. Electron Spectroscopy Techniques

Studies of Dopant Redistribution During Oxide Growth: Phosphorus Pileup — When a thermal oxide is grown on a silicon substrate doped with phosphorus, the phosphorus segregates and piles up on the silicon side of the interface. The presence of phosphorus at the interface increases the oxide growth rate. In addition, the silicon is more heavily doped near the interface than in the bulk, thus affecting device parameters. Study of the pileup phenomenon yields insights into both the oxidation kinetics of silicon and the nature of the silicon-silicon dioxide interface.

The phosphorus density near the interface was measured by means of the crater-edge profiling technique [32]. The test specimens were uniformly doped <111> silicon wafers on which oxide films had been thermally grown.[†] The results of this work [33] showed that the peak density of phosphorus was much higher than the value predicted from diffusion-redistribution theory. The phosphorus peak was also found to be quite narrow, on the order of 4 nm. The phosphorus density in the oxide was below the detectability limit.

Table 1 — Results of Study of Effect of Phosphorus on Measured Width of Silicon-Silicon-
Dioxide Interfaces.

Wafer	Bulk Phosphorus Density, cm^{-3}	10- to 90-Percent Width, nm		50-Percent Width, nm	Peak Phosphorus Density, cm^{-3}
		Oxygen KLL	Silicon LVV		
U	1.0×10^{15}	4.1	2.95	1.55	undetectable
D	5.1×10^{19}	4.7	3.55	1.4	1.3×10^{21}
E	7.2×10^{19}	4.5	3.4	1.35	2.1×10^{21}
F	1.8×10^{20}	4.45	3.05	1.35	2.6×10^{21}
G	2.8×10^{20}	4.5	3.25	1.45	2.6×10^{21}
H	3.2×10^{20}	4.8	3.7	1.6	3.2×10^{21}
J	3.2×10^{20}	5.1	3.75	1.7	2.7×10^{21}

These wafers were recently reexamined to determine if the apparent width of the interface is affected by the presence of phosphorus. The experiments were performed using a 1-μA, 4.5-keV electron beam, rastered over a 100-μm by 100-μm square area. Sputtering was performed with 1-keV argon ions. Oxide thicknesses measured on an interferometer were used to establish the sputtering rates. Profiles of the silicon LVV and oxygen KLL signals were taken. The 10- to 90-percent widths, uncorrected for escape depth, are presented in table 1. The widths between the 50-percent points of these profiles are also tabulated. The measured interface width is seen to increase somewhat with increased phosphorus doping.

Crater-edge profiles were also performed. The approximate phosphorus peak density was determined for each profile by comparison with the bulk silicon peak-to-peak height. These densities are also given in table 1. Interestingly, the bulk silicon peak-to-peak height was also observed to increase with increased doping.   (S. Schwarz,[§] C. R. Helms,[§] and W. E. Spicer[§])

Limitations on Interface Width Resolution in Auger-Sputter Profiling: Ion Knock-On Effects — A simple model of ion knock-on broadening has been developed. This model is based on an analogy to thermal diffusion theory [34]. Broadening is found to occur in rms fashion:

$$W_o = \sqrt{W_m^2 - W^2} , \qquad (8)$$

where W_o is the actual width of the interface, W_m is the measured width, and W is the broadening parameter.

At low energies ($E \leq 1$ keV), it was found that

$$W = \left(\frac{E}{6E_d S}\right)^{1/2} d , \qquad (9)$$

where E is the energy transferred to the solid by the incident ion; E_d is the energy required to displace an atom from its lattice position; S is the sputter yield (the number of atoms sputtered per incident ion), a directly measurable quantity; and d is the nearest-neighbor-distance of the atoms in the solid. The energy dependence of W is rather weak because S increases as E increases. The sputtering yield dependence indicates that, for two different bombarding ions of the same energy:

$$\frac{W_1}{W_2} = \left(\frac{S_2}{S_1}\right)^{1/2} . \qquad (10)$$

At higher energies (1 keV < E < 10 keV), the following semi-empirical formula was found to be appropriate for cases where the electronic energy losses of both the incident ion and the lattice (or dopant) atoms are small:

$$W = \left(\frac{\gamma}{3S}\right)^{1/2} \frac{R}{2} , \qquad (11)$$

where $\gamma = 4M_1 M_2 (M_1 + M_2)^{-2}$, M_1 is the mass of the incident ion, M_2 is the mass of the lattice (or dopant) atom, and R is the ion range.

This model was compared [34] with reasonable success against Monte Carlo calculations and SIMS data reported in the literature and with Auger sputter profile measurements made with several primary ions on the interface between silicon and a thermally grown silicon-dioxide film. The most important attribute was the variation of the broadening parameter, W, with the sputtering yield, S. Profiles were observed to broaden in rms fashion.

(S. R. Schwarz [§] and C. R. Helms [§])

4.3. Use of the Scanning Electron Microscope for Total Dose Testing [¶]

Reliable prediction techniques for the radiation survivability of semiconductor devices in an ionizing radiation environment based on preirradiation measurements have not been established. For this reason, total dose screening of sample devices is frequently employed as part of a hardness assurance program. The kilovolt electron beam in a scanning electron microscope (SEM) has been used in many experiments to explore the effects of ionizing radiation on semiconductor devices and to examine its applicability to hardness screening. This technique has been of interest for hardness assurance because of its convenience and because devices can be selectively irradiated directly at the wafer level. A study of the problems associated with using an SEM in a hardness assurance program to simulate total dose testing with a gamma source such as ^{60}Co has been completed [35].

At least three factors must be considered in order to simulate a ^{60}Co radiation exposure in an SEM. First, for a kilovolt electron beam, the depth-dose distribution through the oxide may be quite different from the assumed constant depth-dose distribution for ^{60}Co exposure. A method for estimating the total absorbed dose in critical oxides has been developed [36]. This method is based on an empirical expression for electron energy dissipation as a function of electron energy and penetration depth [37].

Second, the dose rate during a typical SEM exposure can be considerably higher than typical ^{60}Co dose rates. Third, an SEM properly adjusted for imaging using secondary electrons does not deliver a laterally uniform electron flux to the specimen. In addition, there are practical problems associated with device positioning, device biasing, and possible damage to adjacent devices. All of these considerations are important for ade-

quately specifying SEM total dose testing procedures.

It was concluded that the SEM can serve as a convenient tool for total dose testing of semiconductor devices if attention is given to: (1) the depth-dose distribution of kilovolt electrons and how it relates to the device structure and (2) achieving a uniform electron exposure. The ability to adjust the dose rate delivered in the SEM offers the advantage of being able to deposit a significant dose in a short time period. This technique has unique features in that devices can be selectively irradiated directly at the wafer level, thus saving packaging and possibly bookkeeping costs usually associated with a total dose screen. Also, the radiation sensitivity of different regions of an integrated circuit can be separately investigated. Possible problems, such as application of bias to the device under test, are certainly surmountable.

If the procedures for utilizing the SEM for total dose testing are carefully planned in view of the characteristics of the instrument and the kilovolt electron beams employed, the SEM provides a powerful tool for hardness assurance screening. Programs requiring wafer level traceability should particularly benefit from the application of this technique.

(K. F. Galloway and P. Roitman [#])

5.1. Calibration Standards for Optical Linewidth Measurements on Photomasks

The initial collaborative (pilot) study (NBS Spec. Publ. 400-38, p. 27) to evaluate procedures for measuring 1- to 10-μm wide clear and opaque lines viewed with transmitted illumination was completed [38]. In a blind study, each of three major manufacturing firms in the microelectronics industry received one NBS photomask-like target from the same production batch. Without knowledge of the NBS-measured linewidth values, each of seven groups among the three firms measured selected lines with their own optical microscope using their own non-NBS calibration standards, but following (to widely varying degrees of exactness) NBS directions for performing the measurements. The values which each company group measured for nominally 3-μm wide lines, expressed relative to the NBS measured value (normalized to a value of 3.00 μm), are given in table 2. The differences between company and NBS values are actual observed differences for measurements on the same line and target. Different companies measured different targets; different groups within a company measured the same line on the same target.

Although six of the seven groups used automatic TV-microscope systems (which can give highly reproducible results), the discrepancies between companies, between divisions of the same company, even between groups of the same division of the same company, can be seen from the table to be very large. The appearance of these discrepancies in measurements by technologically advanced and metrologically sophisticated companies points up the serious nature of the linewidth measurement problem.

The pilot study also yielded data for 1- and 10-μm wide lines. Analysis of the results suggests that: (1) the "discrepancies" in linewidth measurements reported to NBS are recurrent and systematic; (2) the discrepancies appear in the results of the most sophisticated microelectronics companies; (3) automatic TV-type systems are as susceptible to systematic errors as visual eyepiece systems; and (4) the discrepancies are not simple constant "offset" types; although complex, they are describable in terms of the phenomena of optical imaging near the resolution limit of the microscope.

Although there is ample evidence that the use of appropriate measurement procedures and calibration artifacts will substantially reduce systematic errors in the measurement system [39] (NBS Spec. Publ. 400-38, pp. 28-29), the results of the present study demonstrate the prevalence of a type of systematic error which cannot be eliminated by the expediency of a "two-point" calibration technique. To overcome the limitations of the present artifact, a new pattern [40] has been designed for use in the next phase of the evaluation which involves NBS and ten industrial laboratories. (D. A. Swyt,* F. W. Rosberry,* and D. Nyyssonen†)

5.2. Spatial-Filtering Microscope

In the previous development of the concept of a spatial-filtering microscope (NBS Spec. Publ. 400-29, pp. 48-50) [41], emphasis was placed on the accurate measurement of small lines and spaces. This was a natural result of the thrust of the current studies which are concerned with improving the accuracy and precision of linewidth measurement. However, in a great many measurement applications, particularly in locating objects within a field that is well-outlined, it is often useful to measure from the edge of the field to somewhere in the inner region. As in measurement of linewidth, this is an asymmetric measurement, the accuracy of which may be improved by use of the spatial-filtering method. It is, therefore, useful to study the effects of band-pass filtering on the images of edges.

The general analysis closely follows the previous study; namely, calculate the spectrum of the complex object, multiply the spectrum by the function that describes the spatial filter, Fourier transform the product, and complex square the result. The resulting expression is the filtered image located in the image plane of the microscope objective.

Figure 7 contains plots of calculated image distributions for a diffraction-limited, 0.50 numerical-aperture (N.A.) objective with filtering (10 cycles per millimeter lower cutoff frequency) and without filtering. The original edge object is shown for comparison. The upper cutoff frequency is determined from the diffraction-limited properties of the lens at

---

*NBS Optics and Micrometrology Section, Mechanics Division.

†NBS Optical Physics Division.

Table 2 — Example of Results Obtained in Pilot Linewidth Measurement Study.[a]

| Type of Measurement | Company A | | | Company B | Company C | | | NBS |
| | Div. 1 | | Div. 2 | | Div. 1 | | Div. 2 | |
	Group 1	Group 2	Group 3		Group 1	Group 2	Group 3	
Width of Clear Space, μm	2.98	2.95	2.75	2.82	3.00	2.76	3.36	3.00
Width of Opaque Line, μm	2.97	3.50	3.31	3.19	3.10	3.12	3.19	3.00
Spacing of Two Lines, μm	5.98	5.99	-	-	5.99	-	5.96	6.00

[a] Different companies measured different targets; different groups within a company measured the same line on the same target. Measured linewidths were normalized to NBS measurements on the same line and target.

a wavelength of 500 nm. This plot clearly illustrates the efficacy of the technique for locating edges.

In general, the results of this study show that: (1) for a given lower cutoff frequency, the width of the dip, or zero, becomes smaller as the numerical aperture of the objective increases and thereby defines the edge location more precisely; and (2) for a given numerical aperture, the larger the lower cutoff frequency, the less energy is

Figure 7. Calculated luminance distributions for filtered and unfiltered images. (A: original edge of object; B: coherent image of edge; C: filtered image of edge. The optics used consist of a 0.50 N.A. objective with a calculated upper cutoff frequency of 1000 cycles/mm at an illumination wavelength of 500 nm. The lower cutoff frequency for the filtered image (curve C) is 10 cycles/mm. The abscissa units are micrometers. Unit magnification is assumed.)

available in the image, but the smaller is the width of the dip. For a 0.50 N.A. objective with a lower cutoff frequency of 80 cycles per millimeter, the image energy in the region about the edge is less by an order of magnitude than that obtained with a cutoff frequency of 10 cycles per millimeter. Since any band-pass filter provides accurate edge location, provided there is sufficient energy left in the image for observation, it is not necessary to employ an optimum filter [45] as it is in measuring narrow lines.

The remaining problem is that of determining the width of a line beyond which it is possible to treat it as a set of two independent edges. The solution of this problem has a bearing on the determination of the upper limit on the use of a spatial-filtering microscope and will also help to delineate the general measurement precision associated with asymmetric optical measurements.

(R. E. Swing[*])

5.3. Primary Linewidth Calibration

In making linewidth determinations in the scanning electron microscope (SEM), the actual measurement of width is based on interferometry in which the location of each edge of the line is obtained from the SEM output. In the model currently being used [42] (NBS Spec. Publ. 400-38, pp. 40-43), the line edge is taken to be a linear ramp, rising at an angle ϕ from the substrate to a thickness t, and the incident electron beam is assumed to

---

[*] NBS Optics and Micrometrology Section, Mechanics Division.

have a Gaussian distribution of electrons. The model also reflects the material characteristics of the edges to be studied; for black-chromium edges, there are three areas of concern: the substrate, the sloped face, and the bulk of the edge. These three regions have different secondary-electron emission coefficients (SEEC) which must be taken into account.

In the previous work which was concerned with a chromium film (covered with a very thin layer of chromium oxide) on a glass substrate, the mid-point on the steep portion of the output was designated as the edge location, since early calculations showed that the mid-point was related to the origin in the edge model. Because this relationship is only approximately true for most cases, it is appropriate to extend the analysis. For the ideal model, the minimum value of the secondary-electron current, I_{min}, is equal to $2\sigma_1$, where σ_1 is the SEEC of the glass substrate. The maximum current, I_{max}, occurs at a value of x given by

$$x = \frac{x_1}{2} + \frac{\ln A}{2x_1} , \qquad (12)$$

where $x_1 = t \cot \phi$, $A = [(\sigma_3 \sec \phi) - \sigma_1]/[(\sigma_3 \sec \phi) - \sigma_2]$, σ_3 is the SEEC of the chromium (in the transition region of the edge), and σ_2 is the SEEC of the chromium oxide (at the other side of the edge). The edge location is taken as the beginning of the slope of the edge ($x = 0$); the current at this position is given by

$$I(0) = (\sigma_1 + \sigma_2) + [(\sigma_3 \sec \phi) - \sigma_2] \text{ erf } x_1 . \qquad (13)$$

The ratio, R, of $I(0)$ to I_{avg} $[= \frac{1}{2}(I_{max} + I_{min})]$ can be calculated. It is a function of the three SEECs, ϕ, and t. Values of R as a function of beam diameter, d, and ϕ are listed in table 3 for the case where the beam diameter is assumed to be that within which 80 percent of the beam energy is contained, $\sigma_1 = 1.000$, $\sigma_2 = 1.265$, $\sigma_3 = 1.030$, and $t = 120$ nm. Use of this model is illustrated in figure 8. I_{avg} is found by averaging the maximum and minimum values of current. $I(0)$ is calculated as the product of I_{avg} and R (found in this case from table 3 for $d = 65$ nm and $\phi = 75$ deg); and the position of the edge is located by dropping a perpendicular line from the $I(0)$ point on the curve which fixes the origin of the distance scale.

This model is deficient on two known counts. It fails to account for the "bloom" (which has been shown to occur at high SEM voltages)

and it does not consider the fairing and rounding at the top and bottom of the real edge. A mathematical function that describes the fairing and rounding at the edges could be developed; this function would require additional experimental evidence from scanning electron micrographs for quantification. This approach does not appear to be difficult. However, consideration of bloom is more important.

The effect of bloom on SEM output is twofold: (1) the current in the region just before the steep rise is somewhat depressed and (2) the region following the maximum is filled in. These effects are illustrated in figure 9. Similar effects have been observed in experimental secondary-electron current curves [42] (NBS Spec. Publ. 400-38, figure 39b). It has been shown that the shape of the curve in the region from which the determination of edge location is made is unchanged by these effects, but the suggested use of maxima and minima for locating the edge may need revision; the mean value cannot be expected *a priori* to remain constant.

The physical phenomena associated with bloom seem clear enough. When the scanning beam is located in the plane regions of constant thickness (before and after the edge discontinuity), a stable system is established so that the flow of secondary electrons is constant for these regions. As the beam approaches the edge from the lower end, the bloom generates electrons that are scattered sidewise under the edge and are prevented from reaching the detector; that is, some of the secondary-electron energy is trapped, thus depressing the current in that region. As the scanning beam moves along the face of the edge, the system again reaches a stable condition until it approaches the top of the edge. There the bloom generates electrons that exit from the top of the edge (in the region of constant thickness, just to the rear of the edge) and cause an apparent increase in secondary-electron energy. As the beam crosses the top of the face and proceeds into the plane region of constant thickness, electrons can now similarly exit from the face near the top, and this behavior results in a slower fall-off in energy than that predicted by the ideal system without bloom.

In the above analysis, it is assumed that the two edges of a line are sufficiently separated so that their interactions with the scanning beam are independent of each other. This is a safe assumption for linewidths of 1 μm and larger. However, since the ongoing

Table 3 — Typical Set of Values of the Ratio, R, of Secondary-Electron Current at Edge Position to Average Secondary Electron Current as a Function of Beam Diameter, d, and Edge Angle, ϕ.

d, nm	ϕ, deg	R
50	50	1.0017
50	55	1.0073
50	60	1.0231
50	65	1.0591
50	70	1.1274
50	75	1.2347
50	80	1.3695
55	50	1.0033
55	55	1.0118
55	60	1.0326
55	65	1.0748
55	70	1.1471
55	75	1.2508
55	80	1.3722
60	50	1.0055
60	55	1.0171
60	60	1.0425
60	65	1.0895
60	70	1.1635
60	75	1.2620
60	80	1.3714
65	50	1.0082
65	55	1.0229
65	60	1.0525
65	65	1.1028
65	70	1.1766
65	75	1.2694
65	80	1.3682
70	50	1.0113
70	55	1.0291
70	60	1.0621
70	65	1.1145
70	70	1.1869
70	75	1.2738
70	80	1.3635

Figure 8. Illustration of the procedure for locating the edge position for a given (calculated) SEM output.
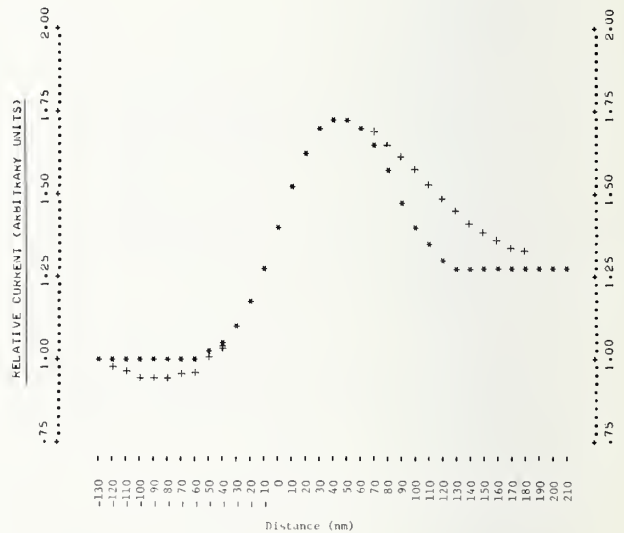
Figure 9. Effects of "bloom" on the (calculated) SEM output of an edge. (The crosses (+) show the modification of the ideal output [shown by the asterisks (*)] for a given amount of "bloom.")

study of submicrometer linewidths must subsequently be considered, it is necessary to formulate expressions for closely spaced edges analogous to those for an isolated edge. The procedure for locating the position of the edge (cf. fig. 8) needs no revi-

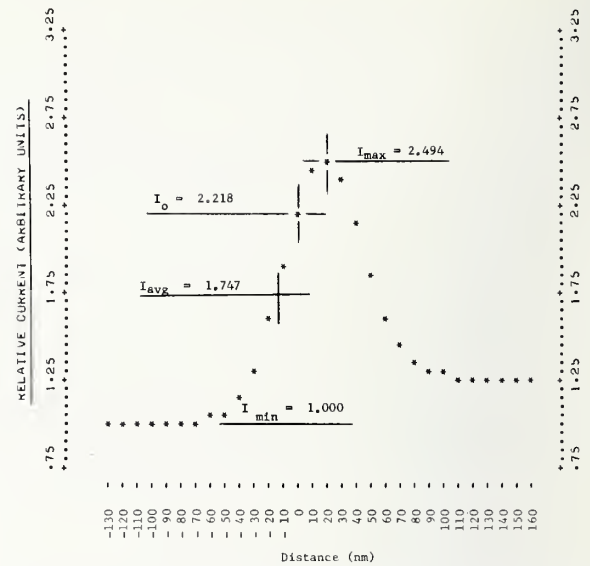sion for application to linewidth, provided there are no perturbing effects between the edges. Typical results are shown in figure 10. Linewidth formulae can also be modified to account for an asymmetric line in which the angles on each edge differ or the materi-

Region:

I   II   III   IV   V
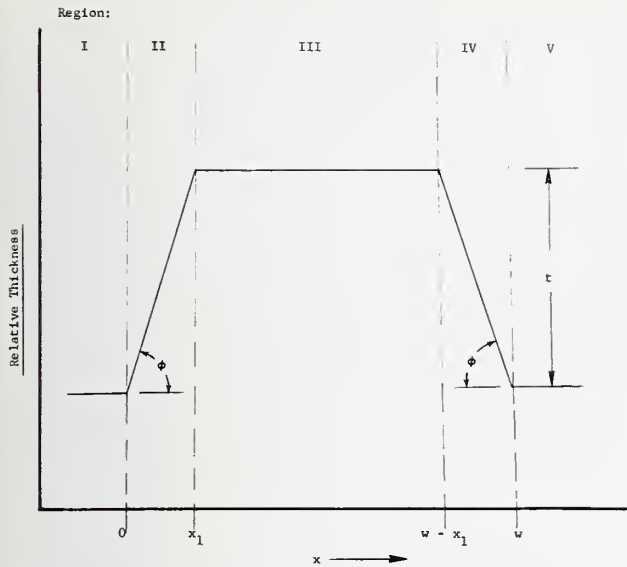
a. Model of a line with width w and showing the thickness parameter t, angles on each face, σ_1 and σ_2, and the five regions with secondary-electron emission coefficients as noted.

b. Calculated SEM output for a line with w = 300 nm, d = 40 nm, t = 110 nm, $\phi_1 = \phi_2 = 55°$, σ_1 = 1.000, σ_2 = 1.265, and σ_3 = 1.026.

Figure 10. Model profile and calculated SEM output trace for a line of width w = 300 nm.

al in the center section of the line is of nonuniform thickness.   (R. E. Swing*)

5.4. Submicrometer Linewidth Measurement[§]

Measurements in Transmitted Light — The NBS transmitted-light linewidth-measurement sys-

tem is a partially coherent system imaging with a 0.90 numerical aperture (N.A.) objective. A theoretical model of the system was developed, and the image profiles computed from this model were shown to be in good agreement with experimental results [43,44]. Although the system was originally developed for measurements in the 1- to 10-μm regime, it was shown theoretically that the method of edge detection could produce accurate measurements for 0.5-μm wide lines and spaces (NBS Spec. Publ. 400-38, pp. 36-40).

A chromium-on-glass photomask[¶] was used to test the system capability at these submicrometer dimensions. The computed and measured image profiles of nominally 0.5-μm wide lines and spaces are shown in figure 11. Because of the unequal widths of the lines and spaces in the experimental traces, the theoretical and experimental data cannot be superimposed. The experimental traces show the period of the multiple 0.5-μm lines to be within a few percent of 1.0 μm, while the chromium lines appear narrower than the spaces with a line-to-space ratio of approximately 0.8. The measuring system has been shown to have a three-sigma precision of +0.025 μm when measuring good quality black-chromium masks with nominally 1.0-μm wide lines and spaces. Sufficient data are not currently available to establish the precision of the measurements on the specimen used in this present study. It appears, however, that the raggedness in the edges determines the repeatability of measurements.

Further theoretical calculations were also made to test the sensitivity of the measuring system to small changes in line and space widths at these dimensions. Figure 12 shows typical calculated image profiles. In all cases, the equation used for the threshold for edge detection [45]:

$$T_c = 0.25 \ (1 + T_o + 2\sqrt{T_o} \ \cos\phi) \ ,$$

where T_o is the relative transmittance of the nearly opaque region and ϕ is the phase difference between the transparent and nearly opaque regions, yields the correct line or
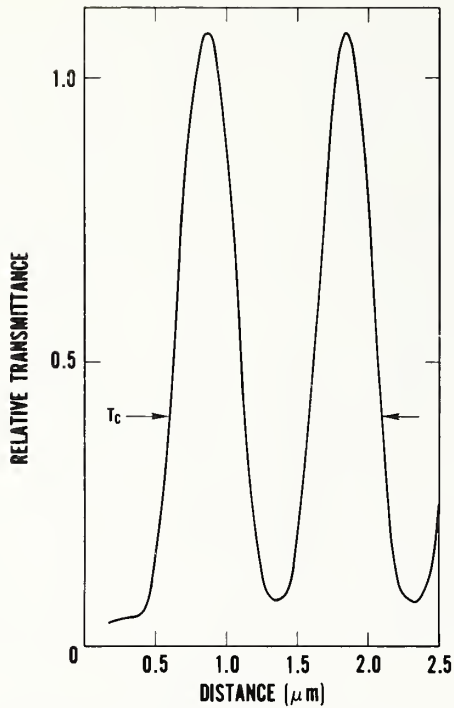
a. Image profile on a bright chromium photo-mask as seen by NBS linewidth measuring system.
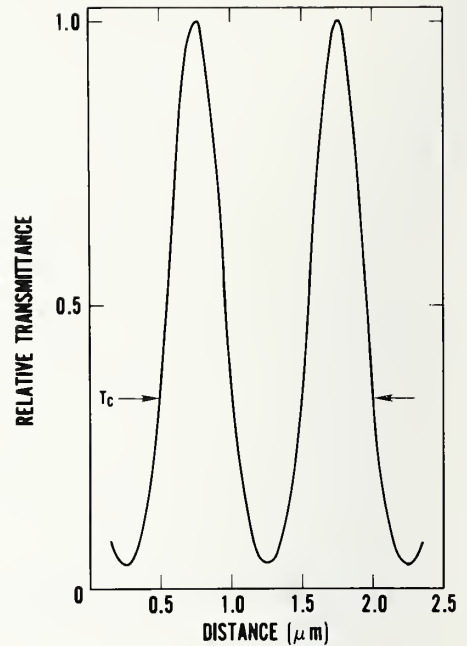
b. Computed image profile based on model of the NBS transmitted-light linewidth measuring system (background transmittance of 2.5% [no phase difference]).

Figure 11.   Computed and measured image profiles of nominally 0.5-μm wide lines and spaces in a chromium-on-glass photomask.
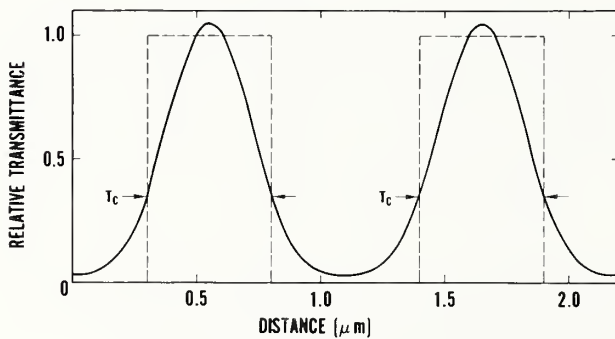
a. $T_O = 0.025$; $\phi = 0$ rad.
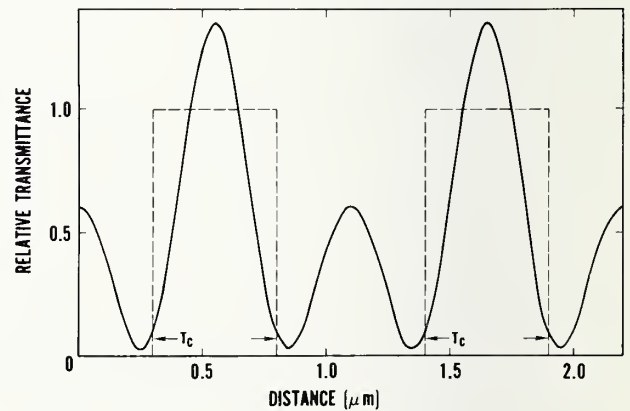
b. $T_O = 0.31$; $\phi = \pi$rad.

Figure 12.   Computed image profiles of multiple line object with 0.5-μm wide lines and 0.6-μm wide spaces.

18

space width to within 1 percent.
(D. Nyyssonen[+] and E. C. Kintner[#])

Measurements in Reflected Light — The reflected-light system (NBS Spec. Publ. 400-38, pp. 33-34) was modified by insertion of a fixed circular aperture in place of the leaf aperture diaphragm which controlled the illuminating numerical aperture. When used with the bright-field reflector, this modification produces the reflection analog of the transmitted-light linewidth-measurement system with the ratio of condenser N.A. to objective N.A. equal to 0.25; this ratio is required for artifacts which produce phase differences of up to π rad on reflection.

Image profiles produced with this reflected-light system have very poor signal-to-noise ratio (S/N). In addition, all of the specimens examined, including resist on wafers, showed differences in spectral reflectance between the substrate and the patterned layer; for example, the substrate may appear yellow-green and the patterned layer, blue-green. An analysis of this effect shows that a thin-film phenomenon effectively makes the specimen appear to differ in contrast with illumination wavelength. Accurate linewidth measurements in reflected light require a

much narrower spectral bandwidth than was needed for the transmitted-light system.

A brief analysis of the reduction of S/N for the reflected-light system as compared with the transmitted-light system shows: (1) there is a reduction factor of 20 or more in S/N because of the lower reflectance of the wafer (typically 4-percent reflectance for the wafer as compared with 90-percent or more transmittance for the photomask); (2) there is an additional reduction factor of 7 in going from 0.66 to 0.25 for the ratio of condenser N.A. to objective N.A.; (3) the beam splitter in the bright-field illumination system introduces another reduction factor of 4; and (4) reducing the spectral bandwidth introduces at least another reduction factor of 6. The transmitted-light system has an S/N ratio of better than 400/1. The losses in the reflected-light system yield an S/N ratio of about 1/10. Since 100/1 is probably the lowest reasonable value required for a good measurement system, the enormous increase in brightness required can only be achieved by use of a laser. Since optimum optical performance of the system requires a wavelength of 530 nm, a krypton laser operating at this wavelength is currently being incorporated in the system.[x]   (D. Nyyssonen[+])

[+]NBS Optical Physics Division.

[#]NBS-NRC Postdoctoral Research Associate, NBS Optics and Micrometrology Section, Mechanics Division.

[x]The system has since been satisfactorily operated with the laser source; see reference [46].

6. TEST PATTERNS

6.1. Random Fault Test Structures

This study was undertaken to evaluate experimentally various ways of determining process-induced wafer defect densities from measurements on the random fault test structures which are included on test pattern NBS-7 [47] (NBS Spec. Publ. 400-29, pp. 65-66). This pattern was designed to be fabricated by a junction-isolated bipolar process, typical of that employed for making transistor-transistor logic (TTL) integrated circuits. The pattern contains three random fault test structures: metal-step-coverage, contact-to-resistor, and multi-emitter-transistor structures.

Since the wafers measured in this study were especially prepared to exhibit a wide range of defect densities, it is possible to observe the effect of the magnitude of the mean defect density on the results obtained by several different methods. This permits an evaluation of various methods of analysis used to estimate the defect density, the degree of success of using reduced testing schemes, and the suitability of the test structures as they exist on test pattern NBS-7 for evaluating a wide range of defect densities.

The metal-step-coverage test structure consists of four segments of 6-μm wide metal runs crossing over cuts in the oxide layer. The segments cross over 46, 92, 253, and 713 oxide cuts, respectively. The presence of a fault was indicated by an open circuit in a particular segment when a current source attempted to drive a 100-mA current through the metal run. The probe pads were large enough to allow two probes to make contact with each pad. This enabled Kelvin-type measurements to be made in order to prevent resistance at the current carrying probe contact from interfering with the potential measurement and also enabled a check to be made to ensure that both probes were contacting the pad, thus avoiding a fault indication due to poor probe contact.

The contact-to-resistor test structure consists of four segments containing a total of 180 diffused p-type resistors of minimum dimensions connected in series with 18-μm wide metallization. All the resistors of the entire structure are located in a common isolation region. Metal probe pads connected to the structure divide the resistor string into four segments containing 12, 24, 72, and 252 resistor contacts, respectively. The pres-

ence of a fault was indicated by an open circuit, rectification greater than 20 percent, or nonlinearity indicating a difference of greater than 20 percent between the resistances measured at applied voltages of 5 and 10 V across the resistor string. Moderate variation in the absolute value of the resistance was not used as a fault indicator since in most instances this was caused by variations in the sheet resistance of the diffused layer across the wafer. As in the case of the metal-step-coverage structures, the probe pads were large enough to permit two probes to make contact with each pad.

The multi-emitter-transistor test structure consists of nine transistors grouped in a common collector region. The base region of each transistor contains either 1, 2, 4, 9, 16, 36, 72, 140, or 286 emitter diffusions. The emitters (24-μm by 24-μm mask dimensions) are arranged in regular rows and columns with a 24-μm spacing between emitters. For each transistor, a probe pad is connected to the base regions and another probe pad is connected to a large metallized area connecting together all the emitters of that transistor. A single probe pad provides contact with the common collector region of the structure. A fault in this test structure results in either an emitter-collector pipe (a low resistance path between the emitter and the collector) or a leaky junction (a short between the base and emitter or base and collector). In practice, a fault was indicated by a collector-emitter breakdown voltage with the emitter shorted to the base (BV_{CES}) of less than 10 V at a current of 10 μA.

For a random distribution of defects on the wafer such that equal areas have an equal probability of intercepting a defect, the probability of a given test structure intercepting a defect is given by the binomial distribution [48]. Let D equal the mean defect density, A equal the area of the test structure susceptible to the defect, and N equal the total number of test structures on the wafer. For $N \gg 1$, the binomial distribution can be approximated by the Poisson distribution to give the following equation for the yield Y [49]:

$$Y = e^{-AD} . \tag{14}$$

Therefore, for a large enough sample of test structures N, the defect density D can be found from the slope of the plot of the natural log of yield against area A. For the case of the metal-step-coverage test structures, it was convenient to let A equal the

20

number of oxide steps crossed by the metal run. For the contact-to-resistor and multi-emitter transistors, A is taken to be the number of contacts in a test segment or the number of emitters in the test transistor, respectively. The four segments of the contact-resistor test structure allow the following combinations of resistor contacts: 12, 24, 36, 72, 84, 96, 252, 264, 296, and 360. By adding together the test results of segments from adjacent test sites in blocks of 2, 4, and 8 test sites, the following combinations of resistor contacts can be added to this list: 48, 144, 192, 288, 504, 576, 720, 1008, 1440, 2016, and 2880. Similar lists of combinations of the number of steps and number of emitters can be generated from the test segments present in the metal-step-coverage and multi-emitter-transmitter test structures.

For a random distribution of defects, the most rigorous method for estimating the defect density involves the measurement of Y for all the possible values of A generated by combining results from segments of individual test sites and blocks of adjacent test sites, followed by determination of the slope of the ln Y-A plot. This procedure is designated method I in the discussion which follows. This procedure tends to be rather time-consuming, so several simplifications of this method were also studied.

An obvious simplification is to reduce the number of combinations of A's by limiting them to the combinations found at each test site. This approach is referred to as method II. A possible problem with method II occurs when the defect density D is very small in relation to the maximum number of test entities (contacts, steps, or emitters, etc.) present in each test site. Under such conditions, it is possible that defects will only be encountered by the largest test segment, and it would be impossible to plot the natural log of yield as a function of A.

A third method works well under the condition where the product of the defect density and the total number of entities at the test site is small, the condition where method II might fail. Method III involves the use of an approximation to eq (14) in order to obtain the defect density estimate directly from the failure rate F [50] which is the complement of the yield:

$$F = 1 - Y .\qquad(15)$$

Using a power series expansion of the exponential function, and retaining only the first two terms of this series, one obtains a simple expression for the defect density:

$$D = F/A .\qquad(16)$$

Since the power series expansion is an alternating series, the error in terminating it at the second term is no greater than the third term in the series. The error in this method should be small if the failure rate is small; for F less than 0.3, the expected error is less than 10 percent. For simplicity, A was taken to be the total number of test entities in the test structure. Then, the failure rate F is that fraction of the test sites of a particular size which contain at least one defect.

These three methods involve testing all of the segments of each test structure with the test pattern stepped and repeated to cover the entire wafer. Three other methods involved data from only a portion of the wafer to see how much the estimates of defect density would change if the number of measurements was substantially reduced. In methods IV and V, only the results obtained from measurements on the largest segment of each test structure were used. In method IV, the defect density was obtained from the slope of the plot of lnY *versus* A (the areas employed are nA_{max}, where n = 1, 2, 3, or 4 and A_{max} is the number of entities in the largest segment of each single test structure), and in method V it was calculated from eq (16). In method VI, D was calculated from eq (16) using only the data gathered from five selected test sites on the wafer. The five sites chosen consisted of one at the center and four located symmetrically about the center approximately two-thirds of the distance from the center to the outer edge of the wafer. Since an average wafer contained 200 usable test sites, method VI represents a very substantial reduction in testing time. This arrangement is intended to simulate the placement of a limited number of test pattern sites on a product wafer.

These six methods of estimating the defect density are compared in table 4 for 10 wafers covering a wide range of defect densities. Wafers 1X, 2Y, 3θ, and 228 were produced using normal processing, whereas the rest of the wafers were produced with processing intentionally altered to induce defects. This was done to be able to evaluate the performance of the test structures over a considerable range of defect densities. The first column of the table contains the wafer identification numbers, arranged in order of increasing defect density as determined by

21

Table 4 — Comparisons of Defect Densities as Estimated by Six Methods.

Wafer Number	Method I D, defects/unit	Percent Difference from Result Obtained by Method I				
		Method II	Method III	Method IV	Method V	Method VI

a. Metal-Step-Coverage Test Structure

Wafer Number	Method I D, defects/unit	Method II	Method III	Method IV	Method V	Method VI
228	7.47×10^{-5}	-15.8	-17.4	+ 1.74	-13.7	-142
3θ	8.21×10^{-5}	- 0.5	+17.8	-55.9	+ 9.26	-
1X	8.6×10^{-5}	-33.7	+14.5	0.0	-14.5	-
2Y	1.03×10^{-4}	- 8.7	- 2.9	- 6.7	- 8.7	-
425 S-11	4.70×10^{-4}	-12.3	-14.7	-14.9	- 0.85	+ 61.4
425 S-12	5.93×10^{-4}	-24.0	+12.9	+ 5.2	+ 0.5	-145
425 S-10	6.15×10^{-4}	- 5.8	+28.9	+59.8	+10.4	-
425 S-3	1.26×10^{-3}	- 3.8	+42.0	+ 2.3	+28.1	- 15.0
425 S-2	1.60×10^{-3}	- 0.6	+47.5	-53.0	+49.4	- 69.0
425 S-4	1.67×10^{-3}	+14.9	+54.0	- 1.2	+38.9	+ 45.8

b. Contact-to-Resistor Test Structure

Wafer Number	Method I D, defects/unit	Method II	Method III	Method IV	Method V	Method VI
1X	8.24×10^{-5}	+48.3	-28.6	+13.6	+ 21.8	-
3θ	1.30×10^{-4}	-43.0	-59.0	- 8.45	-111.0	-
228	1.67×10^{-4}	+44.5	+19.2	-41.4	- 15.0	-
2Y	1.68×10^{-4}	+10.1	-40.5	+32.0	- 22.7	-288.0
425 S-11	1.30×10^{-3}	+ 7.8	+19.2	+22.7	- 8.45	+ 14.6
425 S-12	1.32×10^{-3}	- 6.81	+ 4.55	+25.0	- 22.0	-195.0
425 S-10	1.57×10^{-3}	+23.6	+22.9	- 0.63	+ 7.0	-
425 S-5	2.14×10^{-3}	+12.6	+33.2	+ 6.1	+ 7.48	-137.0
425 S-4	2.35×10^{-3}	- 0.42	+29.8	+ 8.90	+ 8.52	- 25.5
425 S-3	3.13×10^{-3}	-24.9	+32.2	+ 2.7	+ 6.6	+ 1.5

c. Multi-Emitter Transistor Test Structure

Wafer Number	Method I D, defects/unit	Method II	Method III	Method IV	Method V	Method VI
1X	1.66×10^{-4}	+36.1	+36.8	-49.4	- 1.81	-
3θ	2.51×10^{-4}	+26.3	+13.9	+56.5	+ 4.0	-
228	2.90×10^{-4}	+ 1.0	+11.7	+10.0	-24.1	-143.0
2Y	3.67×10^{-4}	0.0	+ 9.6	- 5.18	+12.5	- 92.2
425 S-3	9.98×10^{-3}	- 6.2	+77.0	-	+65.9	+ 29.1
425 S-5	1.1×10^{-2}	- 2.7	+60.0	-	+69.0	+ 18.8
425 S-11	1.21×10^{-2}	+ 3.3	+45.5	-	+71.4	+ 24.0
425 S-12	1.27×10^{-2}	-11.8	+86.5	-	+72.0	+ 33.0
425 S-4	1.62×10^{-2}	-15.4	+89.0	-	+78.5	+ 56.0
425 S-10	1.71×10^{-2}	+ 0.6	+89.5	-	+79.5	+ 52.5

$$\text{Percent difference} = 100 \frac{D \text{ (Method I)} - D \text{ (Other Method)}}{D \text{ (Method I)}}$$

method I, listed in the second column. Columns three through seven contain values of the percent difference between the defect density obtained from method I and that obtained by method II, III, IV, V, or VI, respectively. A dash is used to indicate that the method of analysis failed to give any estimate of the defect density.

It is most instructive to look at the results of each method of estimating the defect density (a given column) for all three test structures. In method II (column 3), yield data for those values of A obtained by combining segments of adjacent test sites is not considered. This eliminates the largest A values, so one would expect to see a significant difference from method I when the defect density is small and the total number of entities per test site (number of entities in the test structure) is small. This problem is evident for the contact-to-resistor test structure. This structure has only 360 contacts per test site compared to 566 emitters for the multi-emitter structure and 1104 steps for the metal-step-coverage test structure.

Method III (column 4) which just uses the failure rate F of the entire test structure agrees only moderately well with method I for wafers with low defect densities. An increasing discrepancy between method I and method III with increasing defect density is clearly evident for the two test structures with the largest number of entities.

Except in the case of the multi-emitter transistor test structure, the results of methods IV and V, which use the test results from only the largest segment of the test structures, agree quite well with the defect density estimate of method I. These methods suffer large errors when the defect densities are large, especially when the number of entities in the largest segment of the test structure is also large. For method IV, once the defect density is large enough that adjacent test sites always have at least one defect in the largest segments, it is not possible to plot the yield *versus* A using information from only the largest segment of the test structure, so no estimate is possible under these conditions. These results indicate that it is not necessary to have a test structure containing segments with different numbers of entities to obtain good estimates of the wafer defect density, provided that the defect density is small enough for the above approximations made to the yield formula to be valid.

In most cases, method VI, where only five sites on the wafer are tested, gives rather unsatisfactory results. When the defect density was low, often none of the five test structures contained a defect, so that no estimate of the defect density could be obtained. In those cases where defects were detected, the density varied considerably from that given by method I.

All of the above six methods of analysis rely on the assumption that the defects causing the test structures to fail are randomly distributed point defects. To investigate the validity of this assumption, the spatial variation of defects was investigated. To estimate the angular dependence, each wafer was divided into nine wedges, each with an angle of 40 deg. The total number of defects within each wedge was counted, and this number was normalized with respect to the largest number of defects found in any wedge on the wafer. Although there was considerable variation in defect density, especially for those wafers which had the smallest defect densities, there appears to be no clear evidence for any overall angular dependence.

The radial dependence of defect density was investigated by dividing the wafer into two regions, separated by a circle with a radius equal to two-thirds of the radius of the wafer. The number of defects was counted for each area and divided by the number of test pattern sites within that area. In the case of the metal-step-coverage test, there seems to be no evidence for a radial dependence of defect density. The results are markedly different for the contact-to-resistor and multi-emitter transistor test results. For these structures, the number of defects per test site for the outer portion of the wafer is consistently greater than the number of defects per test site for the inner portion. The assumption of a random distribution of defects does not seem to be valid for the defects causing the faults in the contact-to-resistor and multi-emitter test structures. It appears that more realistic values of the defect densities could be found by analyzing the two regions of the wafer separately, assuming a random distribution of defects within each region.

In the preceding discussion, nothing has been said about estimating the degree of confidence one can have that the defect density, obtained by even the most rigorous of the six methods used, is very close to the actual value of the wafer defect density. In general, when the number of failures in M defect
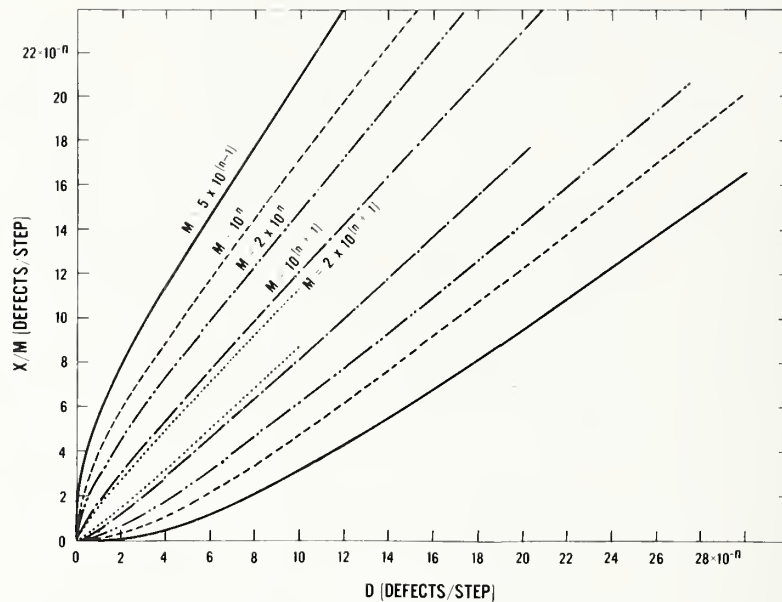
Figure 13. Confidence limits for the defect density D for a confidence level of 95 percent. (X is the number of faulty entities found in a sample of M entities.)

monitors (M resistor contacts, for example) is measured, one can estimate the defect density as the quotient of the number of defective monitors found and the total number of monitors tested. This is exactly what one is doing when using method III, provided that each failure of a test site is due to only one defect. The quality of this estimate depends on the magnitude of the defect density and the size of the sample M. If a random distribution of defects can be assumed, the number of faults encountered by a sampling of N monitors follows a binomial distribution. The statistical charts of the confidence limits for the binomial distribution can be used to answer questions such as: (1) If x defective entities were found in a sample of M entities, what are the 95-percent or 99-percent confidence intervals for the wafer defect density? or (2) For a given range of defect densities, what sample size is required to provide a desired degree of confidence in the estimation of wafer defect density? The statistical charts for the confidence limits of the binomial distribution as derived by Clopper and Pearson [51] do not cover the range of values encountered in this study. Fortunately, under the condition of a large sample size (total number of entities on the wafer) and a small defect density, the binomial dis-

tribution may be approximated by the Poisson distribution. Therefore, the statistical tables of Molina [52] may be used to extend the statistical charts for the confidence limits to range of defect densities desired. Figure 13 presents a version of the extended statistical charts for the 95-percent confidence intervals. The abscissa represents the defect density value multiplied by 10^n where n is a positive whole number greater than one. (For n less than one, the statistical charts of Clopper and Pearson [51] may be used.) The ordinate represents the fraction of defective entities found in the total number of entities examined, multiplied by 10^n. The quantity M is the total number of entities examined; for example, it would equal the total number of contacts per test structure times the total number of test structures measured for the contact-to-resistor test structure. The quantity X is the total number of defects found on the wafer. The two lines labeled with the same M numbers represent for a given X/M ratio the upper and lower bounds of the corresponding defect density values at the 95-percent confidence level. In drawing M items at random from a larger population of mean defect density D, the number of defective items X in the sample will, in general, be different

each time a sample is taken. However, the X/M ratio will be inside the interval between the 95-percent confidence limits, 95 times out a hundred, in the long run of sampling.

To illustrate the use of this chart, consider the metal-step-coverage test results in table 4 for wafer number 228. The fraction of bad steps in the total number tested is found from method III results. Using the percent difference formula and method I defect density, this number is given by $D = X/M = 8.7 \times 10^{-5}$. To use figure 13, let n equal 5. Since there are 1104 steps per test site and approximately 200 test sites per wafer, the sample size M is approximately 2×10^5. With X/M equal to 8.7×10^{-5}, the 95-percent confidence limits on the defect density are read from figure 14 as 5.1×10^{-5} to 1.23×10^{-4} or the defect density can be expressed as $8.7 \pm 3.6 \times 10^{-5}$ at the 95-percent confidence level.

Figure 13 can also be used to see why method VI which used the test results from only five sites yields unsatisfactory results. For five test sites, the sample size is M $\approx$ 5000. Although the 95-percent confidence interval lines are not shown in the figure, they would lie outside the 5×10^4 lines, so for a given X/M ratio, there is a very wide range in the possible values of the defect density.

It should be mentioned that in using figure 13 in conjunction with the results of method III it must be assumed that each faulty test segment found contains no more than one fault. The figure is based on a separate examination of each test entity. However, if the defect density is low and the number of entities per test segment is small enough that the occurrence of multiple faults per test segment is rare, then figure 13 may be used. (G. C. Taylor)

25

7.1. Wire-Bond Pull Test

The wire-bond pull test is the most widely accepted method for controlling the quality of the wire bonding operation and thereby offering added assurance that semiconductor devices will not fail in the field due to weak wire bonds. Specific test procedures and pull-force values are called out in military and other device purchase specifications and yet, until the present study, there has never been a carefully controlled interlaboratory comparison of this important test.

The variables known to affect the bond pull test including ones that cannot be treated theoretically, such as bond peeling and tearing, have been summarized elsewhere [53,54], and ASTM standard procedures for both the destructive [55] and nondestructive [56] bond pull tests have been adopted by the American National Standards Institute.

An interlaboratory comparison (ILC) was carried out under the auspices of ASTM Committee F-1* to verify the destructive bond pull method [55] and to develop data on its reproducibility. For this comparison, all bonds were made with the same bonding machine by the same operator in order to minimize the effect of uncontrolled variables. One substrate was prepared for each of seven participants in the experiment other than NBS.[†]

The bonding substrates were 1.5-in. (38-mm) diameter silicon wafers on which a 0.8- to 1.0-μm thick film of silicon dioxide was thermally grown. A film of aluminum 0.7 to 0.8 μm thick was evaporated onto the oxide and subsequently sintered. The aluminum was patterned in square bonding pads 0.005 in. (0.13 mm) on a side spaced 0.005 in. apart over the entire surface to yield approximately 15,000 pads on each wafer. Each wafer was mounted on a steel base for rigidity and ease of handling.

An ultrasonic bonding machine was set up using previously developed methods [57]. The machine parameters were optimized for bonding in each desired bond-quality group on samples from the same wafer lot and then verified on each individual test wafer. Wire bonds were made with 0.0010-in. (25-μm) diameter, stress-relieved, aluminum 1-percent silicon wire from the same production lot, having a breaking load of 12 to 14 gf.[§] A bond-to-bond spacing of 0.04 in. (1.0 mm) was chosen so that the center of the loop would be over an unused bonding pad, making it easy for the

bond pull operator to center the pulling hook in the bond loop. The center-position loop height was chosen to be 0.011 to 0.012 in. (0.28 to 0.30 mm) in order to minimize the effect that slight variations in loop height or bond-to-bond spacing would have on the resulting pull force. This geometry also yields pull-force values that are the same as the force in the wire at the break point so that no calculation is required to satisfy the referee method [55]. A scanning electron micrograph of a part of a substrate including typical bonds used in the interlaboratory comparison is shown in figure 14.

In order to determine whether there could be any dependence of the precision of the pull-force data on bond quality (e.g., weak or cracked bond heels could be damaged by bond loop movement during accidental misplacement of the pulling hook), the test substrates contained bonds in three quality groups. The first group was prepared to represent high-quality bonds and contained approximately 100 bonds designed to have a mean pull force of approximately 10 gf with a standard deviation, s_x, less than 1 gf. The second group consisted of approximately 100 average-quality bonds designed to have a mean pull force of approximately 7.5 gf with $s_x \sim 1$ gf. The third group consisted of poorly made, overly deformed bonds designed to have a mean pull force of approximately 4 gf with $s_x \sim 1.5$ gf. Because of the large variability, this group contained approximately 200 bonds so that the data obtained would be statistically meaningful.

Because test samples were made on different days and the characteristics of the wire used and the production techniques may have varied somewhat from day to day, these samples may

---

*Committee F-1 on Electronics of the American Society for Testing and Materials, 1916 Race Street, Philadelphia, PA 19103.

[†]The participating organizations were Aerospace Corporation, Bell Telephone Laboratories, Cominco American, Fairchild Semiconductor Corporation, Hewlett-Packard Corporation, Johns Hopkins Applied Physics Laboratory, National Bureau of Standards, and Rockwell International Corporation.

[§]Nearly all measuring gages are calibrated in grams-force. The preferred SI unit for force in this range is the millinewton (mN); 1 gf = 9.8 mN.
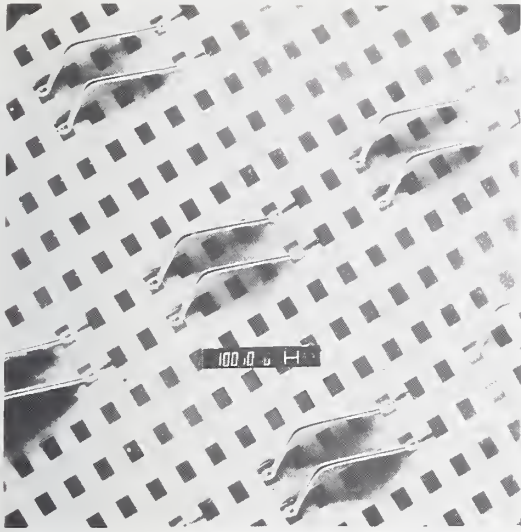
Figure 14. Scanning electron micrograph of typical bonds on a substrate used in the bond pull test interlaboratory comparison. (The bonding pads are square; the rectangular appearance is an artifact resulting from the angle of incidence of the electron beam.)
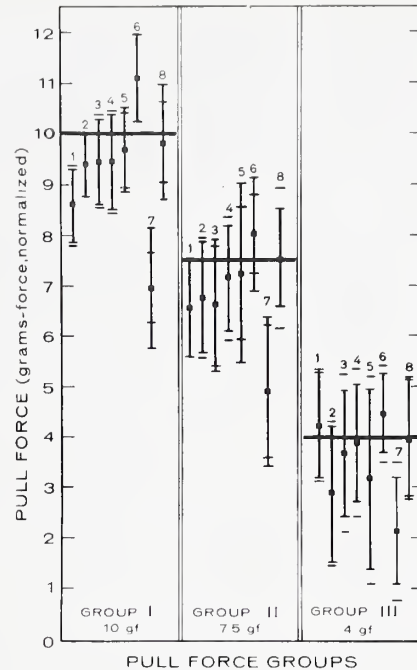

Figure 15. Graphical presentation of the wire-bond pull test interlaboratory comparison data. (The numbers are used to represent the various participating laboratories, except 8 which is an NBS retest. Error bars represent +1 standard deviation of the lab data. Horizontal lines not at an end of a vertical line represent +1 standard deviation of the original NBS data on that laboratory specimen. Group I data are normalized to 10-gf, II to 7.5-gf, and III to 4-gf pull force.)

not represent the same statistical population. Also, being performed by different organizations in different locations, test results from different organizations do not necessarily represent data from the same statistical population. Because of these possible differences, the results of test samples in this interlaboratory test could be directly compared only against the results obtained by the originating laboratory on the same sample. Therefore, approximately one half of the bonds in each group on each wafer were pull tested by the originating laboratory, NBS.

The bond pulling apparatus used in the NBS test [57] employed a graphic readout. The pull mechanism is based on a spring deflection type system similar to that used in a gram gage; the readout is accomplished by the use of a transducer whose output is amplified and displayed as a vertical line on an x-y recorder. Ten calibration points, produced by hanging weights on the hook [55], were fitted by a computer-generated polynomial to obtain a best fit calibration curve. Subsequently, all graphical pull data were entered into the same program, automatically converted into grams-force, and analyzed statistically.

Eleven test samples were produced in March and April 1975. The first distribution to the participating laboratories took place at the June 1975 ASTM Committee F-1 meeting held at NBS. Six samples were given to volunteers among the attendees at the interconnection bonding section meeting. One sample was lost, and pull test data from two other samples had to be disqualified as discussed below; two additional samples were distributed at a later date. Before performing the test, some laboratories held their samples for several months; one laboratory held its sample for two years. Thus, some change in the wire properties as well as annealing of the ultrasonically work hardened bond heel could have occurred before the pull tests were performed.

The analysis of the interlaboratory data took place in April and May 1977 after the results from all tests were received. In most cases, the mean value of the original NBS pull data

from each group was within 0.5 gf of the intended value. However, to better compare the laboratory-to-laboratory data, these mean values were normalized to the intended values of 10, 7.5, and 4 gf, and the normalization factors were then used to normalize each appropriate test group from the participating laboratories.

Figure 15 is a plot of the doubly normalized data from all of the laboratories. The wide spread in results indicated that there were serious problems with the ILC. Because of the time lag from production to pulling by the participating organizations, one of the remaining original samples was tested at NBS on June 3, 1977, to determine if aging effects on the pull strength could be responsible. These samples had remained in mechanically protected, nonhermetic containers at room temperature since their production. An extremely careful recalibration of the equipment was carried out before this test, and the results were incorporated in the computer data analysis calibration program. These data are included in figure 16 as the eighth set. It can be seen that there was no significant change in bond pull force due to the 26-month room temperature storage of the wire bonds.[¶] Thus, other reasons had to be found for the sometimes large variations in pull force from the NBS control values.

An examination of data from Laboratory 6 indicated that all values were given in even grams-force. A discussion with the personnel involved revealed that the operator had not received the calibration procedure and in addition had rounded all values up to the next highest gram mark on the scale of the pulling gage. The gram gage was an old one and old gages tend to read higher as the return spring relaxes or is damaged. Thus, these data were disqualified from the ILC.

Data from Laboratory 7 ranged from 30 to 45 percent lower than the reference values. Lengthy discussions with the laboratory personnel as well as examination of the pulling equipment revealed that the static calibration, specified in the ILC instructions and recommended by the pull tester manufacturer, did not correspond with the dynamic readout. Also, the pulling hook occasionally lurched during pulling in a way that was operator dependent, resulting in its displacement from the bond midpoint. These faults were reported to and were subsequently observed by the manufacturer who has since made available a retrofit kit and has redesigned the tester to eliminate these problems. The data from

Laboratory 7 were also disqualified from the ILC.

Examination of the data from the qualified participants (Laboratories 1 through 5), presented in figure 15, shows that the normalized pull-force values were, with only one exception, lower than those of the NBS reference. The test data from the qualified participants were run through a battery of statistical tests. Of these, only the means of Group II were not significantly different in the analysis of variance test. This test assumes that all data came from the same population, which may not have been the case even after the double normalization if unknown pull test variables had been introduced. Perhaps the most useful of the tests are various multiple comparisons of means [58] as shown in table 5. In this table, the lab numbers are grouped according to the results from the Newman-Keuls procedure; the means are grouped according to results from the Scheffé technique. Lines under a group indicate that the means are not significantly different. Of the two tests, the Newman-Keuls is normally the stricter, but in this case must be considered only approximate since its rigorous application requires that each group be made up of the same number of points. The Scheffé technique corresponds with the f-test and indicates that only the means of Group II are not significantly different, which is evidence that unknown pull test variables were encountered in the other two groups. The data from Group III, which had the highest bond deformation (>2.5 wire diameters), show the poorest correlation in this comparison of means.

The precision of the test was estimated on the basis of relative sample standard deviations which were 7.9, 8.1, and 17.2 percent for Groups I, II, and III, respectively.

One conclusion that may be drawn from the above data is that poor, overly deformed bonds give the widest percentage variation in pull test results. When the test procedure and its precision are sources of contention

---

[¶] This conclusion applies to the wire that was used in the ILC, which was stress-relieved (partially annealed) aluminum 1-percent silicon wire. A slight decrease in pull force of hard (unannealed) aluminum wire bonds of similar composition is not ruled out by these results. Very pure wire (e.g., 99.999-percent aluminum) is known to change its hardness with time.

Table 5 — Multiple Comparisons of Means of
Wire-Bond Pull Test Results.[a]

Group I					
Lab:	1	2	4	3	5
Mean:	8.62	9.38	9.41	9.44	9.65

Group II					
Lab:	1	3	2	4	5
Mean:	6.51	6.61	6.74	7.12	7.23

Group III					
Lab:	2	5	3	4	1
Mean:	2.86	3.11	3.63	3.89	4.17

[a]Lab numbers are grouped according to the re-
sults from the Newman-Keuls procedure; the
means are grouped according to results from
the Scheffé technique. Lines under a group
indicate that the means are not significant-
ly different.

between buyer and seller, pull test compari-
sons should not be made using standard pro-
duction devices since these usually contain a
mix of good, average, and mediocre bonds,
often having a variety of bond geometries.
The test should be prepared on a single-level
substrate, rather than in packages, and con-
sist of high quality bonds. If a low pull-
force range is required, then a relatively
low loop-height-to-bond-spacing ratio should
be used rather than overdeformed bonds. The
test results support the conclusion that the
permitted bond deformation should not exceed
two wire diameters for aluminum wire bonds.

(G. G. Harman and C. A. Cannon)
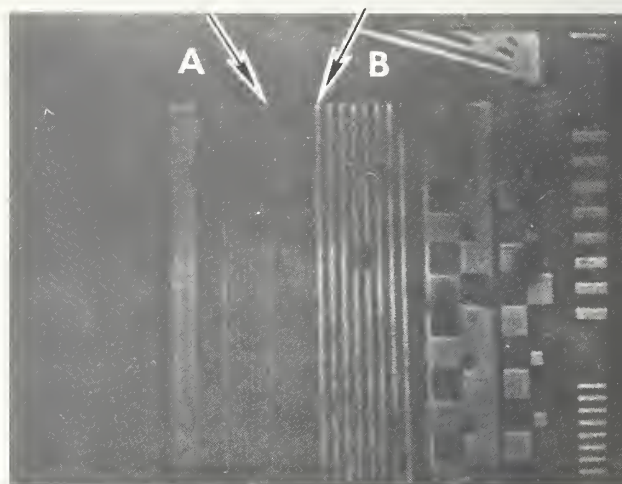
8.1. Scanning Acoustic Microscopy

Spatial Resolution — Experiments were carried
out to study the resolving power of a scan-
ning acoustic microscope (SAM). A resolution
pattern,[*] formed in a 150-nm thick aluminum
film on glass, was used. It contains groups
of equal lines and spaces, 1 and 2 µm wide.
Preliminary results are shown in figure 16.
In the amplitude trace for the SAM operating
at 750 MHz (fig. 16b), the 2-µm wide lines
and spaces are clearly resolved, but the 1-µm
wide lines and spaces are not. In the ampli-
tude trace for an SAM operating at 1100 MHz,
the 1-µm wide lines and spaces are clearly
resolved with an amplitude nearly equal to
that of the 2-µm wide lines and spaces.
(C. F. Quate[†])

Phase Imaging in Reflection — When a polished
surface of a single crystal is examined with
a converging acoustic beam, the reflected
signal has a characteristic response that is
dependent upon the elastic properties of the
reflecting surface [59-61] (NBS Spec. Publ.
400-38, pp. 65-69). For example, consider
the scanning acoustic microscope amplitude
traces shown in figure 17. These long expo-
sure photographs display the variation in the
height of the returning pulses as the test
specimen is translated axially through the
focal point. The triggering of the trace is
such that the horizontal scale on the scope
is a direct measure of the lens-to-specimen
spacing. It is only the upper envelope of
these curves that is significant and the
structure beneath the envelope should be ig-
nored. These curves could be important for
they indicate that the striking differences
in the acoustic response could be used to
monitor the thickness of metallization layers
on silicon. Similar curves are shown in fig-
ure 18 for bare pure surfaces of sapphire,
silicon, and gallium arsenide. These curves
emphasize the striking differences in the re-
sponse of different crystals. (C. F. Quate,[†]
A. Atalar,[†] and H. K. Wickramasinghe[†])

---

[*]Supplied through the courtesy of Bell Labo-
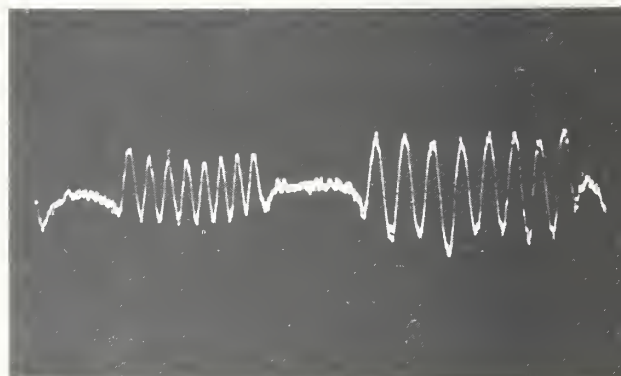ratories.

[†]Work performed at Microwave Laboratory,
Stanford University, under NBS Contract No.
5-35899. NBS contact for additional infor-
mation: R. I. Scace.

a. Scanning acoustic microscope image. A:
1-µm wide lines and spaces. B: 2-µm wide
lines and spaces. f = 1100 MHz.
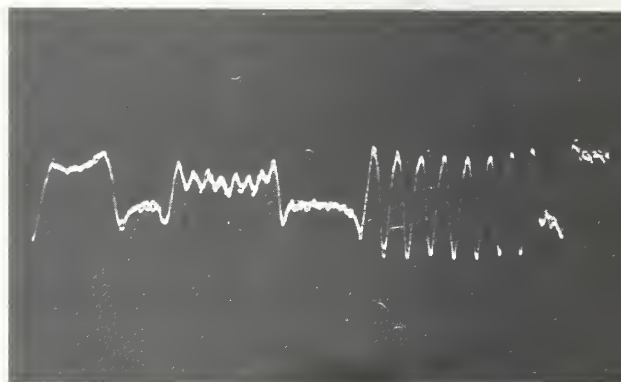
b. Amplitude trace, f = 750 MHz.

c. Amplitude trace, f = 1100 MHz.

Figure 16. Resolution pattern.

a. Bare silicon surface, f = 750 MHz.
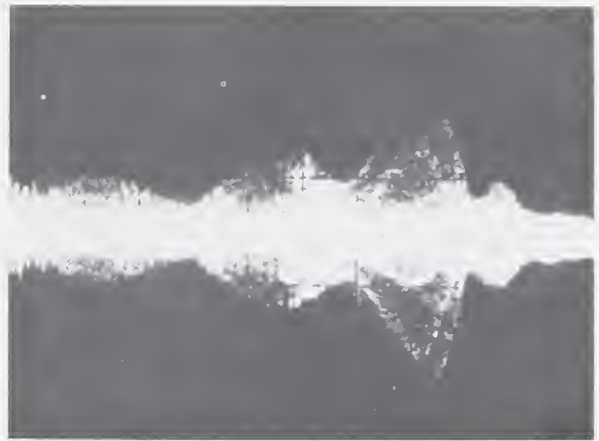
b. Bare silicon surface, f = 1100 MHz.
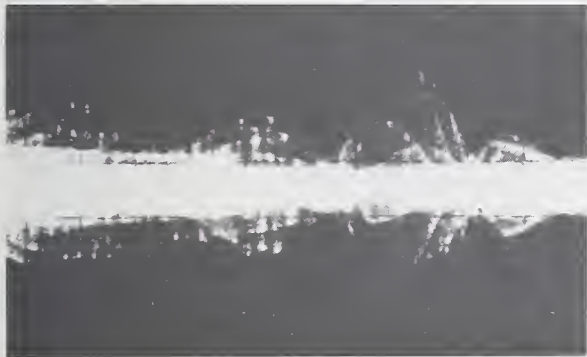
c. A 1-μm thick film of aluminum on silicon, f = 750 MHz.
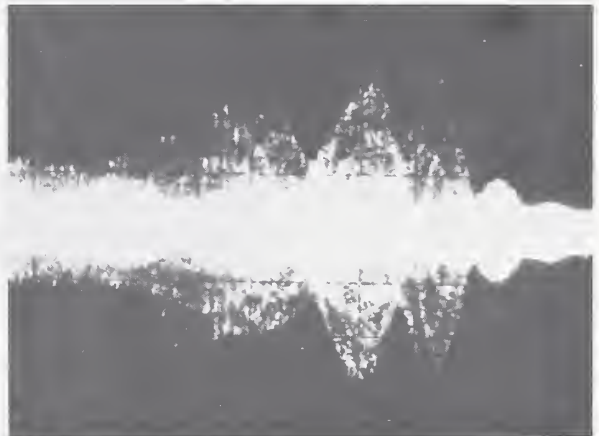
d. A 1-μm thick film of aluminum on silicon, f = 1100 MHz.
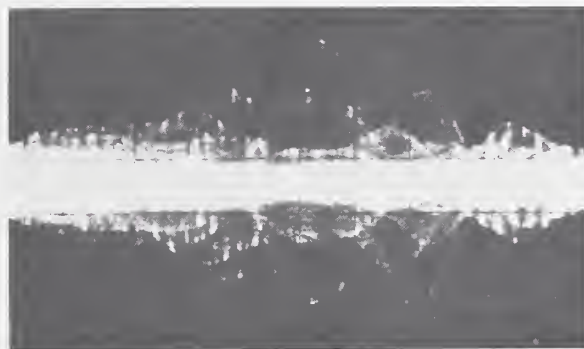
e. A 2-μm thick film of aluminum on silicon, f = 750 MHz.

Figure 17. The amplitude of the SAM output voltage *versus* lens-to-specimen spacing for silicon surfaces as recorded by translating the specimen axially through the focal plane. (The horizontal scale is 3.75 μm/div.)

31
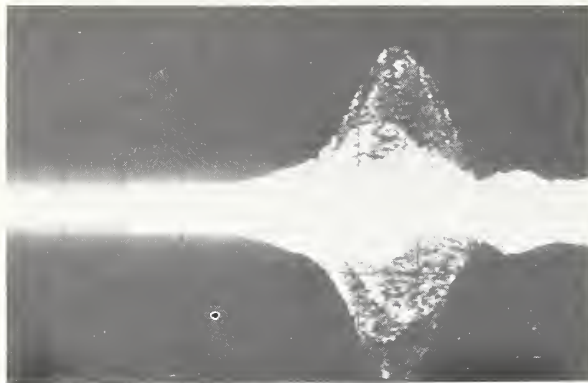
a.   Sapphire.
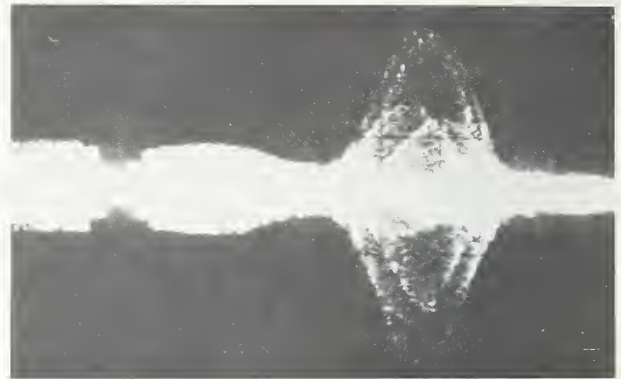
b.   Silicon.
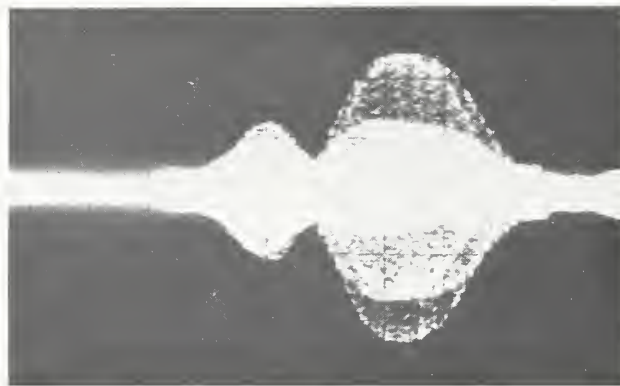
c.   Gallium arsenide.

Figure 18.   The amplitude of the SAM output voltage *versus* lens-to-spacing distances for various crystal surfaces as recorded by translating the specimen axially through the focal plane.   (The horizontal scale is 3.75 μm/div and the signal frequency is 750 MHz.)

Gray Scale — The feasibility of a reflective acoustic gray scale (NBS Spec. Publ. 400-38, pp. 69-70) for operation at 375 MHz was demonstrated [62].   The principle of the technique, useful in calibrating the object-image brightness transfer characteristics of a scanning acoustic microscope, is based on the inherent impedance-matching properties of layers between the immersion liquid (water in this case) and a sapphire crystal substrate. In the demonstration vehicle, a single contoured layer of light borate crown glass was used.   The stair-step pattern in the layers was designed to obtain ten equal increments of power reflection coefficient that cover the available dynamic range of the material system.   The ten-step glass gray scale, fabricated by ion-beam etching, yielded close to a predicted 6-dB bright-to-dark intensity range, with 8 dB representing the upper limit for the materials involved here.   Although the performance was predicted from a plane-wave model, not generally valid in the case of the spherical wavefronts encountered in the highly convergent acoustic beam, the experimentally observed transfer curve was close to predictions.   It was found that the axial position relative to the focal distance, at which agreement was realized, is a function of the material in which the gray scale layer is fabricated.   (R. D. Weglein[§])

9. REFERENCES

1. Li, S. S., and Thurber, W. R., The Dopant Density and Temperature Dependence of Electron Mobility and Resistivity in n-Type Silicon, *Solid-State Electronics* 20, 609-616 (1977).

2. Li, S. S., *Semiconductor Measurement Technology:* The Dopant Density and Temperature Dependence of Electron Mobility and Resistivity in N-Type Silicon, NBS Special Publication 400-33 (March 1977).

3. Li, S. S., The Dopant Density and Temperature Dependence of Hole Mobility and Resistivity in Boron-Doped Silicon, *Solid-State Electronics* 21, 1109-1117 (1978).

4. Li, S. S., *Semiconductor Measurement Technology:* The Theoretical and Experimental Study of the Temperature and Dopant Density Dependence of the Hole Mobility, Effective Mass, and Resistivity in Boron-Doped Silicon, NBS Special Publication 400-47 (November 1979).

5. Sclar, N., Resistivity and Deep Impurity Levels in Silicon at 300 K, *IEEE Trans. Electron Devices* ED-24, 709-712 (1977).

6. Caughey, D. M., and Thomas, R. E., Carrier Mobilities in Silicon Empirically Related to Doping and Field, *Proc. IEEE* 55, 2192-2193 (1967).

7. Irvin, J. C., Resistivity of Bulk Silicon and of Diffused Layers in Silicon, *Bell System Tech. J.* 41, 387-410 (1962).

8. Mousty, F., Ostoja, P., and Passari, L., Relationship Between Resistivity and Phosphorus Concentration in Silicon, *J. Appl. Phys.* 45, 4576-4580 (1974).

9. Wagner, S., Diffusion of Boron from Shallow Ion Implants in Silicon, *J. Electrochem. Soc.* 119, 1570-1576 (1972).

10. Donovan, R. P., and Evans, R. A., Incremental Sheet Resistance Technique for Determining Diffusion Profiles, Silicon Device Processing, C. P. Marsden, Ed., NBS Special Publication 337, pp. 123-131 (November 1970).

11. Buehler, M. G., and Thurber, W. R., A Planar Four-Probe Test Structure for Measuring Bulk Resistivity, *IEEE Trans. Electron Devices* ED-23, 968-974 (1976).

12. Hilibrand, J., and Gold, R. D., Determination of the Impurity Distribution in Junction Diodes from Capacitance-Voltage Measurements, *RCA Rev.* 21, 245-252 (1960).

13. De Mann, H. J. J., On the Calculation of Doping Profiles from C(V) Measurements on Two Sided Junctions, *IEEE Trans. Electron Devices* ED-17, 1007-1008 (1970).

14. Buehler, M. G., Peripheral and Diffused Layer Effects on Doping Profiles, *IEEE Trans. Electron Devices* ED-19, 1171-1178 (1972).

15. Kennedy, D. P., Murley, P. C., and Kleinfelder, W., On the Measurement of Impurity Atom Distributions in Silicon by the Differential Capacitance Technique, *IBM J. Res. Dev.* 12, 399-409 (1968).

16. Kennedy, D. P., and O'Brien, R. R., On the Measurement of Impurity Atom Distributions by the Differential Capacitance Techniques, *IBM J. Res. Dev.* 13, 212-214 (1969).

17. Johnson, W. C., and Panousis, P. T., The Influence of Debye Length on the C-V Measurement of Doping Profiles, *IEEE Trans. Electron Devices* ED-18, 965-973 (1971).

18. Wu, C. P., Douglas, E. C., and Mueller, C. W., Limitations of the C-V Technique for Ion Implanted Profiles, *IEEE Trans. Electron Devices* ED-22, 319-329 (1975).

19. Heald, D., Ordang, P., Skolnik, J., and Nansen, E., Thermodynamics Consideration of p-n Junction Capacitance, *Solid-State Electronics* 16, 655-665 (1973).

20. De Mari, A., An Accurate Numerical Steady State Solution of the p-n Junction, *Solid-State Electronics* 11, 33-58 (1968).

21. Kennedy, D. P., and O'Brien, R. R., On the Mathematical Theory of the Linearly-Graded p-n Junction, *IBM J. Res. Dev.* 11, 252-270 (1967).

22. Oettinger, F. F., Ed., Measurement Techniques for High Power Semiconductor Materials and Devices: Annual Report,

January 1 to December 31, 1977, Department of Energy Report HCP/T6010/A021-02 (September 1978), pp. 51-59.

23. Sah, C. T., Chan, W. W., Fu, H. S., and Walker, J. W., Thermally Stimulated Capacitance (TSCAP) in p-n Junctions, *Appl. Phys. Letters* 20, 193-195 (1972).

24. Buehler, M. G., Impurity Centers in PN Junctions Determined from Shifts in the Thermally Stimulated Current and Capacitance Response with Heating Rate, *Solid-State Electronics* 15, 69-79 (1972).

25. Lang, D. V., Deep Level Transient Spectroscopy: A New Method to Characterize Traps in Semiconductors, *J. Appl. Phys.* 45, 3023-3032 (1974).

26. Buehler, M. G., Investigation of Radiation-Induced Defects in Silicon P-N Junctions, Final Report, AFCRL-72-0578 (1972).

27. Lang, D. V., Fast Capacitance Transient Apparatus: Application to ZnO and O Centers in GaP p-n Junctions, *J. Appl. Phys.* 45, 3014-3022 (1974).

28. Sah, C. T., Forbes, L., Rosier, L. L., Tasch, A. F., Jr., and Tole, A. B., Thermal Emission Rates of Carriers at Gold Centers in Silicon, *Appl. Phys. Letters* 15, 145-148 (1969).

29. See reference [22], pp. 46-49.

30. Buehler, M. G., and Phillips, W. E., A Study of the Gold Acceptor in a Silicon p^+n Junction and an n-Type MOS Capacitor by Thermally Stimulated Current and Capacitance Measurements, *Solid-State Electronics* 19, 777-788 (1976), see Appendix B.

31. Larrabee, G., and Dobrott, R., Techniques for the Preparation and Analysis of Standard Silicon Semiconductor Specimens for the Ion Microprobe Mass Analyzer, NBS-GCR-79-158 (January 1979).

32. Taylor, N. J., Johannessen, J. S., and Spicer, W. E., Crater-Edge Profiling in Interface Analysis Employing Ion-Beam Etching and AES, *Appl. Phys. Letters* 29, 497-499 (1976).

33. Johannessen, J. S., Spicer, W. E., Gibbons, J. F., Plummer, J. D., and Taylor, N. J., Observation of Phosphorus Pile-Up at the SiO_2-Si Interface, *J. Appl. Phys.* 49, 4453-4458 (1978).

34. Schwarz, S. A., and Helms, C. R., An Ion Knock-On Mixing Model with Application to Si-SiO_2 Interface Studies, *J. Vac. Sci. Tech.* 16, 781-783 (1979).

35. Galloway, K. F., and Roitman, P., Important Considerations for SEM Total Dose Testing, *IEEE Trans. Nucl. Sci.* NS-24, 2066-2070 (1977).

36. Galloway, K. F., and Roitman, P., Some Aspects of Using a Scanning Electron Microscope for Total Dose Testing, NBSIR 77-1235 (September 1977).

37. Everhart, T. E., and Hoff, P. H., Determination of Kilovolt Electron Energy Dissipation vs. Penetration Depth in Solid Materials, *J. Appl. Phys.* 42, 5837-5846 (1971).

38. Swyt, D. A., Rosberry, F. W., and Nyyssonen, D., Calibration of Optical Microscopes for Photomask Linewidth Measurements, *Proc. Microelectronics Seminar — Interface '77*, Monterey, California, October 5-7, 1977, pp. 131-144.

39. Swyt, D. A., and Rosberry, F. W., A Comparison of Some Optical Microscope Measurements of Photomask Linewidths, *Solid State Technology* 20 (8), 70-75 (August 1977).

40. Swyt, D. A., Design of a Pattern on a Photomask-Like Physical Standard for Evaluation and Calibration of Linewidth-Measuring Systems, *Solid State Technology* 21 (1), 35-42 (January 1978).

41. Swing, R. E., The Theoretical Basis of a New Optical Method for the Accurate Measurement of Small Line-Widths, *Proc. Soc. Photo-Optical Instrum. Engrs.* 80, *Developments in Semiconductor Microlithography,* 65-77 (1976).

42. Jerke, J. M., Hartman, A. W., Nyyssonen, D., Swing, R. E., Young, R. D., and Keery, W. E., Comparison of Linewidth Measurements on an SEM/Interferometer System and an Optical Linewidth-Measuring Microscope, *Proc. Soc. Photo-Optical Instrum. Engrs.* 100, *Developments in Semiconductor Microlithography II,* 37-45 (1977).

43. Nyyssonen, D., Linewidth Measurement with an Optical Microscope: The Effect of Operating Conditions on the Image Profile, *Appl. Optics* 16, 2223-2230 (1977).

44. Nyyssonen, D., Optical Linewidth Measurements on Silicon and Iron-Oxide Photomasks, *Proc. Soc. Photo-Optical Instrum. Engrs.* 100, *Developments in Semiconductor Microlithography II*, 127-134 (1977).

45. Nyyssonen, D., Optical Linewidth Measurements on Wafers, *Proc. Soc. Photo-Optical Instrum. Engrs.* 135, *Developments in Semiconductor Microlithography III*, 115-119 (1978).

46. Nyyssonen, D., Spatial Coherence: The Key to Accurate Optical Micrometrology, *Proc. Soc. Photo-Optical Instrum. Engrs.* 194, *Applications of Optical Coherence*, 34-44 (1979).

47. Buehler, M. G., and Sawyer, D. E., Microelectronic Test Patterns Aid Production of Custom ICs, *Circuits Manufacturing* 17 (2), 46-56 (February 1977).

48. Stapper, C. H., Defect Density Distribution for LSI Yield Calculations, *IEEE Trans. Electron Devices* ED-20, 655-657 (1973).

49. Lindgren, B. W., and McElrath, G. W., *Introduction to Probability and Statistics*, p. 61 (The Macmillan Company, New York, 1959).

50. Turley, A. P., and Herman, D. S., LSI Yield Projections Based Upon Test Pattern Results: An Application to Multilevel Metal Structures, *IEEE Trans. Parts, Hybrids, and Packaging* PHP-10, 230-234 (1974).

51. Clopper, C., and Pearson, E., The Use of Confidence or Fiducial Limits Illustrated in the Case of the Binomial, *Biometrika* 26, 404-413 (1934).

52. Molina, E. C., *Poisson's Exponential Binomial Limit* (D. Van Nostrand Co., Inc., New York, 1942).

53. Albers, J. H., Ed., *Semiconductor Measurement Technology:* The Destructive Bond Pull Test, NBS Special Publication 400-18 (February 1976).

54. Harman, G. G., and Cannon, C. A., The Microelectronic Wire Bond Pull Test — How to Use It, How to Abuse It, *IEEE Trans. Components, Hybrids, and Manufacturing Technology* CHMT-1, 203-210 (1978).

55. Standard Methods for Measuring Pull Strength of Microelectronic Wire Bonds, ASTM Designation F 459, *Annual Book of ASTM Standards*, Part 43 (November 1979).

56. Standard Recommended Practice for Nondestructive Pull Testing of Wire Bonds, ASTM Designation F 458, *Annual Book of ASTM Standards*, Part 43 (November 1979).

57. Harman, G. G., Ed., *Semiconductor Measurement Technology:* Microelectronic Ultrasonic Bonding, NBS Special Publication 400-2 (January 1974).

58. Snedecor, G. W., and Cochran, W. G., *Statistical Methods*, Chapter 10 (Iowa State University Press, Iowa City, Iowa, 1967).

59. Atalar, A., Quate, C. F., and Wickramasinghe, H. K., Phase Imaging in Reflection with the Acoustic Microscope, *Appl. Phys. Letters* 31, 791-793 (1977).

60. Weglein, R. D., and Wilson, R. G., Characteristic Material Signatures by Acoustic Microscopy, *Electron. Lett.* 14, 352-354 (1978).

61. Atalar, A., An Angular Spectrum Approach to Contrast in Reflection Acoustic Microscope, *J. Appl. Phys.* 49, 5130-5139 (1978).

62. Weglein, R. D., Gray Scale for Scanning Acoustic Microscopy, *Electron. Lett.* 14, 656-657 (1978).

APPENDIX

SEMICONDUCTOR TECHNOLOGY PROGRAM
PROGRESS REPORTS

A review of the early work leading to this Program is given in Bullis, W. M., Measurement Methods for the Semiconductor Device Industry — A Review of NBS Activity, NBS Tech. Note 511 (December 1969).

Progress reports covering the period July 1, 1968, through June 30, 1973, were published as NBS Technical Notes with the title, Methods of Measurement for Semiconductor Materials, Process Control, and Devices:

Quarter Ending	NBS Tech. Note	Date Issued	NTIS Accession No.
September 30, 1968	472	December 1968	AD 681330
December 31, 1968	475	February 1969	AD 683808
March 31, 1969	488	July 1969	AD 692232
June 30, 1969	495	September 1969	AD 695820
September 30, 1969	520	March 1970	AD 702833
December 31, 1969	527	May 1970	AD 710906
March 31, 1970	555	September 1970	AD 718534
June 30, 1970	560	November 1970	AD 719976
September 30, 1970	571	April 1971	AD 723671
December 31, 1970	592	August 1971	AD 728611
March 31, 1971	598	October 1971	AD 732553
June 30, 1971	702	November 1971	AD 734427
September 30, 1971	717	April 1972	AD 740674
December 31, 1971	727	June 1972	AD 744946
March 31, 1972	733	September 1972	AD 748640
June 30, 1972	743	December 1972	AD 753642
September 30, 1972	754	March 1973	AD 757244
December 31, 1972	773	June 1973	AD 762840
March 31, 1973	788	August 1973	AD 766918
June 30, 1973	806	November 1973	AD 771018

After July 1, 1973, progress reports were issued in the NBS Special Publication 400- sub-series with the title, Semiconductor Measurement Technology:

Quarter Ending	NBS Spec. Publ.	Date Issued	NTIS Accession No.
September 30, 1973	400-1	March 1974	AD 775919
December 31, 1973 / March 31, 1974	400-4	November 1974	COM 74-51222
June 30, 1974	400-8	February 1974	AD/A 005669
September 30, 1974	400-12	May 1975	AD/A 011121
December 31, 1974	400-17	November 1975	AD/A 017523
March 31, 1975 / June 30, 1975	400-19	April 1976	PB 251844
September 30, 1975 / December 31, 1975	400-25	October 1976	PB 258555
March 31, 1976 / June 30, 1976	400-29	April 1977	AD/A 040011
September 30, 1976	400-36	July 1978	PB 283482
December 31, 1976 / March 31, 1977	400-38	November 1979	PB 80-120231

36

NBS-114A (REV. 9-78)

U.S. DEPT. OF COMM. BIBLIOGRAPHIC DATA SHEET	1. PUBLICATION OR REPORT NO. Spec. Publ. 400-45	2. Gov't. Accession No.	3. Recipient's Accession No.

4. TITLE AND SUBTITLE Semiconductor Measurement Technology: Progress Report, April 1, 1977 to September 30, 1977	5. Publication Date August 1980
	6. Performing Organization Code

7. AUTHOR(S) W. Murray Bullis, Editor	8. Performing Organ. Report No.

9. PERFORMING ORGANIZATION NAME AND ADDRESS NATIONAL BUREAU OF STANDARDS DEPARTMENT OF COMMERCE WASHINGTON, DC 20234	10. Project/Task/Work Unit No.
	11. Contract/Grant No. See item 15.

12. SPONSORING ORGANIZATION NAME AND COMPLETE ADDRESS (Street, City, State, ZIP) NBS, Washington, DC 20234; SSPO, Washington, DC 20376; DNA, Washington, DC 20305; ARPA, 1400 Wilson Blvd, Arlington, VA 22209; ERDA, Washington, DC 20545; Naval Oceans Systems Center, 271 Cataline Blvd., San Diego, CA 92152	13. Type of Report & Period Covered Interim: Apr. 1, 1977 to Sept. 30, 1977
	14. Sponsoring Agency Code

15. SUPPLEMENTARY NOTES
ARPA Order 2397, Program Code 7D10; DNA IACRO 77-809; SSPO Order N00016476WR70036, Code SP-23; ERDA TAsk Order AO21-EES; Naval Ocean Systems Center Order N0095377MPO9005.

☐ Document describes a computer program; SF-185, FIPS Software Summary, is attached.

16. ABSTRACT *(A 200-word or less factual summary of most significant information. If document includes a significant bibliography or literature survey, mention it here.)*

This progress report describes NBS activities directed toward the development of methods of measurement for semiconductor materials, process control, and devices. Both in-house and contract efforts are included. The emphasis is on silicon device technologies. Principal accomplishments during this reporting period included (1) development of theoretical expressions for computing resistivity and hole mobility for boron-doped silicon; (2) completion of a study of problems associated with use of a scanning electron microscope for total dose testing of semiconductor devices; (3) completion of a pilot study to evaluate procedures for measuring 1- to 10-μm wide clear and opaque lines viewed with transmitted illumination; (4) completion of a preliminary study of test structures for estimating densities of process-induced random faults in device wafers; and (5) completion of an interlaboratory evaluation of the destructive wire bond pull test. Also reported is other ongoing work on materials characterization by electrical and physical analysis methods, materials and procedures for wafer processing, photolithography, test patterns, and device inspection and test procedures.

17. KEY WORDS *(six to twelve entries; alphabetical order; capitalize only the first letter of the first key word unless a proper name; separated by semicolons)*
Capacitance-voltage methods; deep level transient spectroscopy; electrical properties; electron irradiation; electronics; hole mobility; integrated circuits; ion knock-on effect; ion microprobe mass analysis; Irvin's curves; isothermal transient capacitance method; linewidth measurements; measurement technology; microelectronics; phosphorus pileup; photolithography; pull test; random fault test structures; resistivity; scanning acoustic microscope; scanning electron microscope; semiconductor devices; semiconductor materials; semiconductor process control; silicon; silicon dioxide; spatial filtering microscope; sputter-Auger method; test structures; transistors; wire bonds.

18. AVAILABILITY ☒ Unlimited	19. SECURITY CLASS (THIS REPORT)	21. NO. OF PRINTED PAGES
☐ For Official Distribution. Do Not Release to NTIS	UNCLASSIFIED	43
☒ Order From Sup. of Doc., U.S. Government Printing Office, Washington, DC 20402	20. SECURITY CLASS (THIS PAGE)	22. Price
☐ Order From National Technical Information Service (NTIS), Springfield, VA. 22161	UNCLASSIFIED	$2.25

USCOMM-DC

NBS TECHNICAL PUBLICATIONS

PERIODICALS

JOURNAL OF RESEARCH—The Journal of Research of the National Bureau of Standards reports NBS research and development in those disciplines of the physical and engineering sciences in which the Bureau is active. These include physics, chemistry, engineering, mathematics, and computer sciences. Papers cover a broad range of subjects, with major emphasis on measurement methodology and the basic technology underlying standardization. Also included from time to time are survey articles on topics closely related to the Bureau's technical and scientific programs. As a special service to subscribers each issue contains complete citations to all recent Bureau publications in both NBS and non-NBS media. Issued six times a year. Annual subscription: domestic $13; foreign $16.25. Single copy, $3 domestic; $3.75 foreign.

NOTE: The Journal was formerly published in two sections: Section A "Physics and Chemistry" and Section B "Mathematical Sciences."

DIMENSIONS/NBS—This monthly magazine is published to inform scientists, engineers, business and industry leaders, teachers, students, and consumers of the latest advances in science and technology, with primary emphasis on work at NBS. The magazine highlights and reviews such issues as energy research, fire protection, building technology, metric conversion, pollution abatement, health and safety, and consumer product performance. In addition, it reports the results of Bureau programs in measurement standards and techniques, properties of matter and materials, engineering standards and services, instrumentation, and automatic data processing. Annual subscription: domestic $11; foreign $13.75.

NONPERIODICALS

Monographs—Major contributions to the technical literature on various subjects related to the Bureau's scientific and technical activities.

Handbooks—Recommended codes of engineering and industrial practice (including safety codes) developed in cooperation with interested industries, professional organizations, and regulatory bodies.

Special Publications—Include proceedings of conferences sponsored by NBS, NBS annual reports, and other special publications appropriate to this grouping such as wall charts, pocket cards, and bibliographies.

Applied Mathematics Series—Mathematical tables, manuals, and studies of special interest to physicists, engineers, chemists, biologists, mathematicians, computer programmers, and others engaged in scientific and technical work.

National Standard Reference Data Series—Provides quantitative data on the physical and chemical properties of materials, compiled from the world's literature and critically evaluated. Developed under a worldwide program coordinated by NBS under the authority of the National Standard Data Act (Public Law 90-396).

NOTE: The principal publication outlet for the foregoing data is the Journal of Physical and Chemical Reference Data (JPCRD) published quarterly for NBS by the American Chemical Society (ACS) and the American Institute of Physics (AIP). Subscriptions, reprints, and supplements available from ACS, 1155 Sixteenth St., NW, Washington, DC 20056.

Building Science Series—Disseminates technical information developed at the Bureau on building materials, components, systems, and whole structures. The series presents research results, test methods, and performance criteria related to the structural and environmental functions and the durability and safety characteristics of building elements and systems.

Technical Notes—Studies or reports which are complete in themselves but restrictive in their treatment of a subject. Analogous to monographs but not so comprehensive in scope or definitive in treatment of the subject area. Often serve as a vehicle for final reports of work performed at NBS under the sponsorship of other government agencies.

Voluntary Product Standards—Developed under procedures published by the Department of Commerce in Part 10, Title 15, of the Code of Federal Regulations. The standards establish nationally recognized requirements for products, and provide all concerned interests with a basis for common understanding of the characteristics of the products. NBS administers this program as a supplement to the activities of the private sector standardizing organizations.

Consumer Information Series—Practical information, based on NBS research and experience, covering areas of interest to the consumer. Easily understandable language and illustrations provide useful background knowledge for shopping in today's technological marketplace.

Order the above NBS publications from: Superintendent of Documents, Government Printing Office, Washington, DC 20402.

Order the following NBS publications—FIPS and NBSIR's—from the National Technical Information Services, Springfield, VA 22161.

Federal Information Processing Standards Publications (FIPS PUB)—Publications in this series collectively constitute the Federal Information Processing Standards Register. The Register serves as the official source of information in the Federal Government regarding standards issued by NBS pursuant to the Federal Property and Administrative Services Act of 1949 as amended, Public Law 89-306 (79 Stat. 1127), and as implemented by Executive Order 11717 (38 FR 12315, dated May 11, 1973) and Part 6 of Title 15 CFR (Code of Federal Regulations).

NBS Interagency Reports (NBSIR)—A special series of interim or final reports on work performed by NBS for outside sponsors (both government and non-government). In general, initial distribution is handled by the sponsor; public distribution is by the National Technical Information Services, Springfield, VA 22161, in paper copy or microfiche form.

BIBLIOGRAPHIC SUBSCRIPTION SERVICES

The following current-awareness and literature-survey bibliographies are issued periodically by the Bureau:

Cryogenic Data Center Current Awareness Service. A literature survey issued biweekly. Annual subscription: domestic $25; foreign $30.

Liquefied Natural Gas. A literature survey issued quarterly. Annual subscription: $20.

Superconducting Devices and Materials. A literature survey issued quarterly. Annual subscription: $30. Please send subscription orders and remittances for the preceding bibliographic services to the National Bureau of Standards, Cryogenic Data Center (736) Boulder, CO 80303.

SPECIAL FOURTH-CLASS RATE
BOOK